

Artemisinin Cocrystals for Bioavailability Enhancement: Part 2. *In-vivo* Bioavailability and PBPK Modelling

*Manreet Kaur¹, Vanessa Yardley², Ke Wang¹, Jinit Masania¹, Randolph RJ Arroo¹, David B.
Turner³ and Mingzhong Li^{1*}*

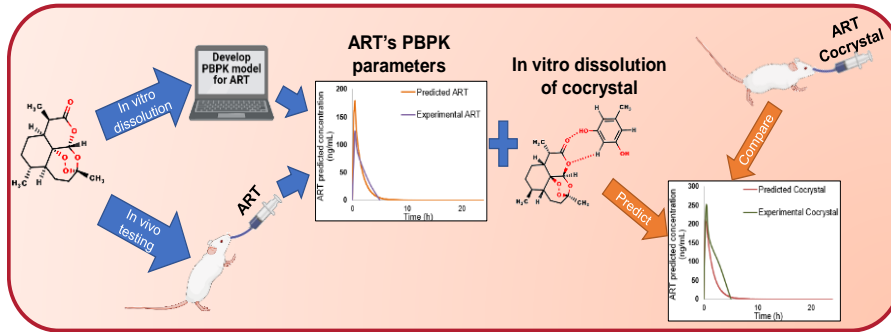
¹Leicester School of Pharmacy, De Montfort University, Leicester LE1 9BH, U.K.

²Department of Infection & Immunity, Faculty of Infectious & Tropical Diseases, London
School of Hygiene and Tropical Medicine, London WC1E 7HT, U.K.

³Certara UK Limited, Simcyp Division, Sheffield, S1 2BJ, U.K.

* Corresponding Author, Tel: +44(0)1162577132; Email: mli@dmu.ac.uk

Table of Contents Graphic



Abstract

We report the evaluation and prediction of the pharmacokinetic (PK) performance of artemisinin (ART) cocrystal formulations, i.e., 1:1 Artemisinin-Orcinol (ART-ORC) and 2:1 Artemisinin-Resorcinol (ART²-RES), using *in vivo* murine animal and PBPK (physiological based pharmacokinetic) models. The efficacy of the ART cocrystal formulations along with the parent drug ART were tested in mice infected with *Plasmodium berghei*. When given at the same dose, the ART-cocrystal formulation showed a significant reduction in parasitaemia at day 4 post infection compared to ART alone. The PK parameters including C_{\max} (maximum plasma concentration), T_{\max} (time to C_{\max}), AUC (area under the curve) were obtained by determining drug concentrations in the plasma using LC-HRMS (Liquid Chromatography-High Resolution Mass Spectrometry), showing enhanced ART levels after dosage with the cocrystal formulations. The dose-response tests revealed that a significantly lower dose of the ART cocrystals in the formulation was required to achieve a similar therapeutic effect as ART alone. A PBPK model was developed using a PBPK mouse simulator to accurately predict the *in vivo* behaviour of the cocrystal formulations by combining *in vitro* dissolution profiles with the properties of the parent drug ART. The study illustrated that information from classical *in vitro* and *in vivo* experimental investigations of the parent drug of ART formulation can be coupled with PBPK modelling to predict the PK parameters of an ART cocrystal formulation in an efficient manner. Therefore, the proposed modelling strategy could be used to establish *in vitro* and *in vivo* correlations for different cocrystals intended to improve dissolution properties and to support clinical candidate selection, contributing to assessment of cocrystal developability and formulation development.

Key words: pharmaceutical cocrystal, artemisinin, pharmacokinetics, parasitaemia, PBPK modelling

Introduction

In the pharmaceutical industry, cocrystallization of active pharmaceutical ingredients (APIs) has become an increasingly important strategy to improve the oral bioavailability of poorly soluble compounds [1]. A pharmaceutical cocrystal is a multi-component crystal comprising two or more compounds (i.e., one is the API and the others are called coformers) that are solids under ambient conditions, are present in a stoichiometric ratio and interact by noncovalent interactions such as hydrogen bonding [2, 3]. API cocrystal screening is now a routine step in early-stage drug development, and several cocrystal-containing drug products, such as Lexapro® - cocrystal of escitalopram oxalate with oxalic acid, and Entresto® - cocrystal of sacubitril and valsartan, are in clinical use [4].

Although pharmaceutical cocrystals can generate dramatic changes in an APIs' physicochemical properties (i.e. solubility and dissolution rates), transformations of these improved properties of cocrystals into drug products with the required pharmacokinetics *in vivo* is not straightforward [5]. Once the cocrystals contact the gastrointestinal (GI) fluid, they start to dissolve, showing often complex behaviour of dissolution, supersaturation and precipitation [6]. To maintain and improve the performance of the cocrystals, addition of a polymer may be required as a nucleation and/or crystal growth inhibitor to prevent parent drug crystallization. Selecting a suitable combination of a cocrystal and polymeric inhibitor is usually accomplished through trial-and-error tests *in vitro* [7-14]. Drug absorption is a highly complex process, which is dependent upon numerous factors, including the physicochemical properties of the drug, characteristics of the formulation, and interplay with the underlying physiological properties of the GI tract, e.g. the pH environment and metabolic enzymes [15]. These *in vitro* tests may not be sufficient to identify an optimal cocrystal from a range of coformers and/or polymeric inhibitors in the formulation because they cannot provide insight into all the mechanisms of GI absorption *in vivo* [16]. Therefore, it is of great importance to

develop formulation strategies for cocrystal products that can be used to accurately predict oral drug absorption *in vivo*.

Physiologically based pharmacokinetic (PBPK) models, that combine physiological and anatomical parameters of living species, physicochemical properties of API and formulation design, offer a mean to predict PK parameters (i.e., Absorption, Distribution, Metabolism Elimination, ADME) of drugs in virtual populations [17, 18]. Currently, PBPK models are increasingly used in formulation development to explore and understand formulation performance [19-26]. For example, the *in vitro* data from dissolution testing with the physicochemical properties of the drug under study, e.g. pKa, solubility, diffusion coefficient and effective permeability, were used as input functions into PBPK models to simulate the *in vivo* profiles of the drug [27, 28]. Within a formulation development PBPK models can also be used to study the food effect [29, 30], dose selection [31], drug-drug interactions (DDIs) through auto-induction of enzymes metabolism [32, 33], contributing to the Replace, Reduce and Refine (3Rs) targets for the use of non-human species in scientific research [34].

This study, for the first time, reports the evaluation and prediction of the pharmacokinetic performance of Artemisinin (ART) cocrystal formulations, i.e. 1:1 Artemisinin-Orcinol (ART-ORC) and 2:1 Artemisinin-Resorcinol (ART²-RES), using *in vivo* murine animal and PBPK models. We illustrate how information from classical *in vitro* dissolution tests and *in vivo* experimental investigations of the parent drug can be coupled with PBPK modelling to predict the *in vivo* performance of cocrystals in an efficient manner.

In this work the ART cocrystal formulations (i.e. ART-ORC and ART²-RES), along with the parent drug ART, were tested in mice infected with *Plasmodium berghei*, a suitable model for studying the aetiology of malaria as the infection presents structural, physiological and life cycle analogies with human disease [35]. In the first part of the study, it was found that a copolymer Polyvinylpyrrolidone/vinyl Acetate (PVP-VA) at 0.05 mg/mL was required within

the formulation to maintain the performance of ART cocrystals [36]. The efficacy of the ART cocrystal formulations was examined by analysis of the percentage parasitaemia of *Plasmodium berghei* in the blood smears taken over the course of four-day treatments at a repeatedly fixed dose of 30 mg/kg ART [37, 38]. A dose-response experiment was then conducted with the most active ART cocrystal formulation from the first mouse study. The formulation was administered at three repeated fixed doses of 3 mg/kg, 10 mg/kg and 30 mg/kg ART for the same course of four-day treatments. The ART plasma concentration-time profiles of the formulations on day 1 (D1) and day 4 (D4) after the repeated dosing of 30 mg/kg were obtained to determine their PK parameters and examine the ART time-dependent PK. Studies have shown that ART is not only poorly soluble in an aqueous environment, resulting in poor and erratic absorption upon oral administration [39], but also markedly induces its own metabolic elimination, leading to decreased plasma levels on repeat dosing [40-44].

A PBPK modelling platform, Simcyp (Mouse Simulator Version 19.1), was employed to simulate the ART plasma concentration-time profiles of an ART cocrystal formulation in the systemic circulation of a mouse [45, 46]. As the first step of the model development, simulations of the oral mouse plasma concentration-time profiles of ART were performed, using *in vitro* dissolution data of the parent drug ART formulation with its physicochemical properties as inputs into the mouse PBPK model. The PBPK model simulations were then compared to the *in vivo* ART plasma concentration-time profiles from animal experiments. This provided a means to refine the model parameters through the parameter sensitivity analysis and parameter fittings, and to verify the PBPK model's predictive ability of the *in vivo* performance of the ART formulation. Through the comparison of the predicted and measured PK parameters, the effectiveness of the PBPK model prediction of the ART cocrystal formulations can be examined.

Materials and Methods

Materials

Artemisinin (ART, 98% purity), resorcinol (RES, >99% purity), santonin (SAN), Drug free mouse serum, potassium dihydrogen phosphate (KH_2PO_4), sodium hydroxide (NaOH), dihydroartemisinin (DHA) and chloroquine hydrochloride (CQ) were purchased from Sigma-Aldrich (Dorset, UK). Orcinol (ORC, 98% purity) was purchased from Fisher Scientific (Loughborough, UK). LCMS (Liquid Chromatography- Mass Spectrometry) grade solvents including methanol, acetonitrile, water and formic acid were purchased from Fisher Scientific and used as received. Double distilled water (DDW) was generated from a bi-distiller (WSCO44.MH3.7, Fistream International Limited, Loughborough, UK) and used throughout the study. A copolymer polyvinylpyrrolidone (60%)/vinyl acetate (40%) (PVP-VA) was gifted by Ashland Inc (Schaffhausen, Switzerland). Electrospray tuning mix for LC-HRMS (Liquid Chromatography-High Resolution Mass Spectrometry) was purchased from Agilent Technologies Ltd (Cheshire, UK).

Methods

Preparation of powdered ART cocrystals

Artemisinin and orcinol cocrystal (ART-ORC) was prepared by a solvent evaporation method. A 1:1 equimolar mixture of ART and ORC was dissolved in the solvent mixture of chloroform and methanol (9:1) at room temperature. The solution was placed in a fume cabinet (room temperature, airflow 0.5-1.0 m/s) for 4-5 days to let the solvents evaporate.

Artemisinin and resorcinol cocrystal (ART²-RES) was synthesized by seeded solvent evaporation methods. A 2:1 molar mixture of ART and RES was used to prepare the seeds of cocrystals by a neat grinding method using Retsch Mixer Mill MM 400 (Retsch, Germany) along with 15mL stainless steel SmartSnap™ jars containing two 7mm stainless steel grinding balls (Form-tech Scientific, Montreal, Canada) for 60 mins. The neat ground cocrystals were then used as seeds to prepare enough ART²-RES needed for experiments by solvent

evaporation method, where a 2:1 molar ratio mixture of both components was present in a saturated cosolvent solution of chloroform and methanol (9:1). The cocrystal solutions were allowed to evaporate in a controlled fume hood for 4-5 days.

Formation of ART cocrystals was confirmed by Powder X-Ray Diffraction (PXRD) and Differential Scanning Calorimetry (DSC).

Phosphate buffer solution (PBS)

PBS at pH 6.8 (0.01M) was used as the dissolution media in this study. It was prepared according to the British Pharmacopeia 2018; 50mL of 0.2M potassium dihydrogen phosphate (KH_2PO_4) and 22.4mL of 0.2M sodium hydroxide (NaOH) were mixed and diluted to 1000mL with DDW.

In vitro dissolution test of an ART formulation

In vitro dissolution tests were conducted on ART formulations in non-sink conditions in pH 6.8 PBS (0.01M) in the absence or presence of a pre-dissolved 0.05 mg/mL concentration of PVP-VA polymer. In order to reduce the effect of particle size on the dissolution rates, ART, ART-ORC and ART²-RES samples were ground using a 60 Mesh sieve to obtain a particle size of <250 μm . The experiments were carried out at $37\pm 0.5^\circ\text{C}$ in a PTWS 120D dissolution apparatus (PharmaTest, Germany) at 50 rpm stirring speed. The total volume of dissolution media was 400 mL, in which 150 mg of ART, 215.9 mg of ART-ORC and 179.3 mg ART²-RES was added. 1 mL sample was withdrawn at sampling times 5, 10, 15, 30, 60, 120, 180 and 240 mins. The withdrawn sample was centrifuged using an MSC 010.CX2.5 centrifuge (MSE Ltd., London, UK) at 13,000 rpm for 1 min. The supernatant was separated, diluted with ethanol and the concentrations were detected using HPLC (High Performance Liquid Chromatography).

HPLC methods for ART, ORC and RES

The sample concentration of ART, ORC or RES in solution was determined by Agilent series 1100 automatic HPLC equipped with a diode array detector. A Roc C18 column (5 μm , 150x4.6

mm, Restek) was used and the column temperature was maintained at 25°C. Details of HPLC methods are shown in Table S1 in the supporting materials. The ART calibration samples were prepared in acetonitrile in a range of 5-50 µg/mL. The ORC and RES calibration samples were prepared in DDW in a range of 5-50 µg/mL. Details of the calibration and validation results are in Tables S2-S3 in the supporting materials.

Pharmacokinetic studies

Female BALB/c mice aged 6 to 8 weeks, at 18-20 g, were purchased from Charles River Ltd (Margate, UK). The mice were ordered one week before the start of experiments. These mice were kept in controlled rooms with humidity of 55% and temperature of 26°C and fed water and rodent food *ad libitum*. The mice were also provided with environmental enrichments to enhance behavioural well-being, such as varied nesting materials and platforms within the cage. The health and well-being of all mice were assessed at least once a day by a trained team of technicians as well as researchers. All efforts were made to minimize the number of animals used and their suffering. At the end of the experiments, all mice were humanely killed.

In this work two Stages of *in vivo* experiments were carried out: (i) Stage 1: to evaluate the PK performances and efficacies of ART cocrystal formulations at a fixed dose of 30 mg/kg over a four-day course of the treatment regimen, and (ii) Stage 2: to evaluate the dose response of the best ART cocrystal formulation at various doses of 30 mg/kg, 10 mg/kg and 3 mg/kg over the same course of the treatment regimen. In order to illustrate the effectiveness of the ART cocrystal formulations, a comparative study with those treated by the ART alone was also carried out. The reference and control of the experiments were the untreated infected mice and those treated by chloroquine (CQ) solution at a fixed dose of 10 mg/kg for the four-day treatment regimen. The CQ solution was selected as a control drug in this study as *Plasmodium berghei* is sensitive to chloroquine [47].

- (i) Infection procedure and drug administration vehicle

Plasmodium berghei NK65 infected blood was collected from infected donor mice and diluted with 0.85% saline to produce an infective inoculum of 1×10^6 infected erythrocytes/mL [48]. The mice for both in vivo experiments were infected with 0.2 mL i.v. and allocated into their respective groups. Two hours post infection experimental groups were treated with different formulations and then treated once a day for a total of 4 consecutive days. The dosing scheme and sample collections are shown in Fig. 1.

According to the formulation development in the first part of the study [36], ART or ART cocrystals were suspended in PBS in the presence of 0.05 mg/mL PVP-VA (copolymer of *N*-vinyl-2pyrrolidone 60% and vinyl acetate 40%) and then administered orally to mice. Chloroquine hydrochloride was dissolved in sterile DDW. All crystalline materials prior to the tests were slightly ground by a mortar and pestle and sieved by a 60 Mesh sieve (particle size $<250 \mu\text{m}$) to reduce the effect of particle size on the dissolution rates.

(ii) Stage 1: Treatment regimens at a fixed dose

The mice were divided into 5 groups in this Stage (detailed in Fig. 1), including Group 1 of untreated mice, Group 2 of mice treated with 10 mg/kg CQ, Group 3 of mice treated with 30 mg/kg ART; Group 4 of mice treated with 30 mg/kg ART-ORC and Group 5 of mice treated with 30 mg/kg ART²-RES. Five mice were used in Groups 1 and 2 to collect blood samples for parasitaemia count only, fifteen mice were used in Groups 3, 4 and 5 to collect the blood samples for both the parasitaemia count and determination of ART concentrations in plasma.

5 mL solutions of 30 mg/kg ART (15 mg in 5 mL), 30 mg/kg ART-ORC (21.6 mg in 5 mL) and 30 mg/kg ART²-RES (17.9 mg in 5 mL) were prepared by suspending appropriate amount of each drug in the administration vehicle. Therefore, all of the formulations have the same amount of ART. 5 mL of 10 mg/kg CQ solution was prepared by dissolving 5 mg CQ into DDW. All of suspensions and solution were freshly prepared daily and gavage dosed to the mice in a 0.2 mL bolus for the course of treatment. The first dose was given 2 hours after the

mice were injected with *Plasmodium berghei*-infected blood from the infected donor mice. The repeated doses were given at the same time for the following days.

During the treatment, the blood samples for parasitaemia counts were collected starting from the second day treatment for 4 days as shown in Fig. 1. A thin smear of blood from the tail vein of a mouse before dosing was made on glass slides which were left to air dry first and then fixed with methanol. The slides were immersed in 10% Giemsa's stain for 10 min and dried after removal of excess stain with water. Five thin smears from five different mice in each group were obtained.

The ART plasma concentration-time profiles in Groups 3, 4 and 5 were determined after dosing of the formulations on the first day (D1) and the fourth day (D4) shown in Fig. 1. The blood sample volume of ~50 μ L was withdrawn from the tail vein of a mouse and placed in an Eppendorf tube at different time points after dosing including 0.25, 0.5, 1, and 3 hrs. The blood samples were allowed to clot by leaving them undisturbed at room temperature for 30 mins. The plasma was separated by centrifugation at 4000 rpm for 10 min at 4°C and was stored at -80°C until analysis. At each of the sampling points, three blood samples from three different mice in each group were taken. Due to the limited blood volume in each mouse, 15 mice were used in each of the test groups so that the blood sample was only taken once over the course of sampling points.

(iii) Stage 2: dose-response experiments

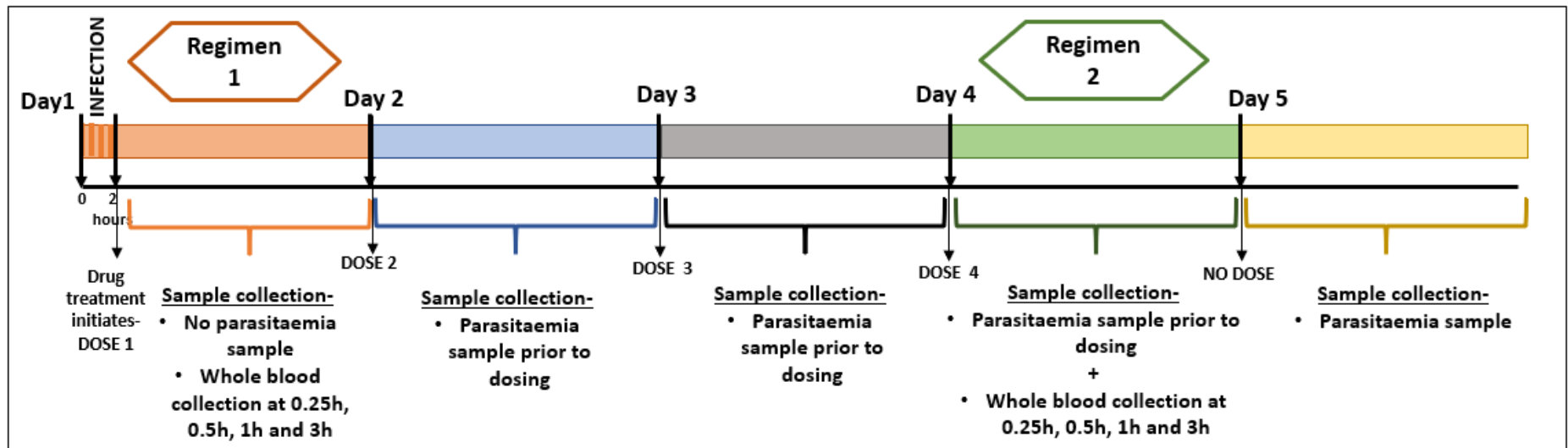
Based on the results from the Stage 1 experiments, an additional dose-response study was carried out on the most active cocrystal formulation, ART-ORC, from the first study. ART and ART-ORC suspensions were prepared at three different concentrations of 30 mg/kg, 10 mg/kg and 3 mg/kg. All of the suspensions were freshly prepared and gavage dosed to the mice in a 0.2 mL bolus every day for 4 days (D1 to D4). The reference and control of the experiments were the untreated infected mice and those treated by CQ solution at a fixed dose of 10 mg/kg

for the four-day treatment regimen. Additionally, dihydroartemisinin (DHA) was also included in the comparative study because it is one of the recommended Artemisinin-based combination therapies (ACTs) by World Health Organisation (WHO) in the treatment of uncomplicated *Plasmodium falciparum* malaria [49], which was prepared in PVP-VA aqueous suspension as a dose of 30 mg/kg.

The administration vehicle for all formulations except CQ was 0.05 mg/mL PVP-VA in pH 6.8 PBS (0.01M). The oral dose volume was fixed as 0.2 mL therefore 5 mL solutions of 30 mg/kg ART (15 mg in 5 mL), 10 mg/kg ART (5 mg in 5 mL), 30 mg/kg ART-ORC (21.6 mg in 5 mL), 10 mg/kg ART-ORC (7.19 mg in 5 mL) and 30 mg/kg DHA (15 mg in 5 mL) were prepared by suspending appropriate amount of each drug in the administration vehicle. 10 mL solutions of 3 mg/kg ART (3 mg in 10 mL) and 3 mg/kg ART-ORC (4.3 mg in 10 mL) were prepared by suspending appropriate amount of each drug in the administration vehicle.

The mice were divided into 9 groups in this Stage (detailed in Fig.1), including Group 1 of untreated mice; Group 2 of mice treated with 10 mg/kg CQ dissolved in sterile DDW; Groups 3-5 of mice treated with 30 mg/kg, 10 mg/kg and 3 mg/kg ART dissolved in administration vehicle respectively; Groups 6-8 of mice treated with 30 mg/kg, 10 mg/kg and 3 mg/kg ART-ORC dissolved in administration vehicle respectively; Group 9 of mice treated with 30 mg/kg DHA dissolved in administration vehicle. During the treatment regimes, the blood samples for parasitaemia counts were collected starting from the second day of treatment for 4 days as shown in Fig. 1. The blood samples for the ART plasma concentration-time profiles were taken for Groups 3 and 6 only. Similarly, the five blood smears in each of 9 groups were daily collected for parasitaemia counts starting from the second day of the treatments. Three blood samples in each of Groups 3 and 4 were collected after dosing on day 1 and day 4 at different time points i.e., 0.25, 0.5, 1, and 3 hours. The dosing scheme and sample collections are shown in Fig. 1.

Fig. 1: Dosing scheme and sampling collection of *in vivo* experiments (i) and (ii)



Stage 1

Group 1- untreated control (n=5)
Group 2, 10 mg/kg CQ in sterile DDW (n=5)
Group 3, 30 mg/kg ART in 0.05 mg/mL PVP-VA solution (n=15)
Group 4, 30 mg/kg ART-ORC in 0.05 mg/mL PVP-VA solution (n=15)
Group 5, 30 mg/kg ART-RES in 0.05 mg/mL PVP-VA solution (n=15)

(n)= number of mice; serum sample from untreated mice were taken to confirm absence of ART in mice serum

Stage 2

Group 1- untreated control (n=5)
Group 2, 10 mg/kg CQ in sterile DDW (n=5)
Group 3, 30 mg/kg ART in 0.05 mg/mL PVP-VA solution (n=15)
Group 4, 10 mg/kg ART in 0.05 mg/mL PVP-VA solution (n=5)
Group 5, 3 mg/kg ART in 0.05 mg/mL PVP-VA solution (n=5)
Group 6, 30 mg/kg ART-ORC in 0.05 mg/mL PVP-VA solution (n=15)
Group 7, 10 mg/kg ART-ORC in 0.05 mg/mL PVP-VA solution (n=5)
Group 8, 3 mg/kg ART-ORC in 0.05 mg/mL PVP-VA solution (n=5)
Group 9, 30 mg/kg DHA in 0.05 mg/mL PVP-VA solution (n=5)

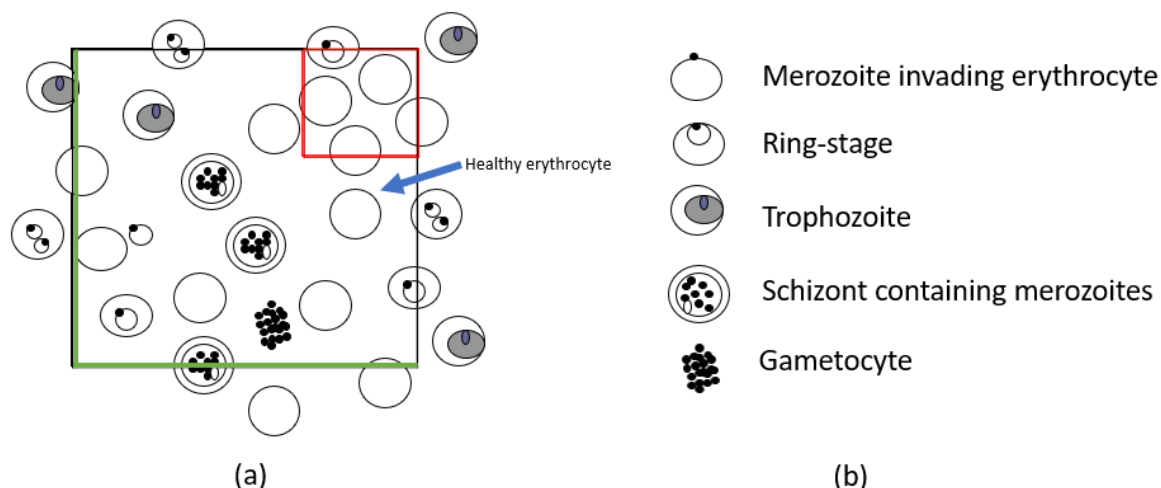
Parasitaemia counts

The percentage parasitaemia of *Plasmodium berghei* was calculated by counting the number of infected and healthy erythrocytes under oil immersion (Zeiss Immersol 518N) at 100X magnification. A region of the slide where the erythrocytes were spaced fairly evenly without excessive overlapping was selected. A counting graticule with 2 squares as shown in Fig. 2 is used to count the cells, where the healthy erythrocytes have round shape and looks like biconcave discs and the parasitized cells are of different shapes under the microscope. The shape of a parasitized cell indicates the stage of infection, detailed in Fig. 2(b). The daughter parasites i.e. merozoites are motile in nature and invade the healthy erythrocytes. The ring stage shows thin, delicate ring of parasite around the cytoplasm and one or two small chromatin dots. The trophozoite stage has a characteristic signet ring with a denser cytoplasm as compared to the young ring-stage. The schizonts have a coarse granular appearance with segments of individual merozoites. The gametocyte is round in shape with a granular appearance and is usually larger than healthy erythrocytes [50].

The healthy erythrocytes were assumed to be uniformly spread on the microscopic slide, therefore, the healthy cells in the small red square, one-ninth area of the big square, were counted, making the counting approach more time-efficient. The parasitized cells inside the large square were counted. As some cells lie on the borders of the squares, any parasitized cells which lied on the two borders in green of the large square were counted. The healthy cells lying on the corresponding two parallel borders of the small red square were also counted. This method allowed a systematic approach to count the cells where repetition in counting was avoided whilst producing accurate and reproducible results. The counting was repeated for different fields of the slide until over 50 parasitized cells or over 200 healthy erythrocytes were reached. Cell Counting Aid software (Monash University, Australia) was used to count the cells in both squares. At least five mice were used per group to calculate %parasitaemia shown in Eq. (1).

$$\%parasitaemia = \frac{\text{number of parasitised cells}}{\text{number of Healthy erythrocytes} \times 9} \times 100 \quad (1)$$

Fig.2: (a) Illustration of one field on the microscopic slide, showing parasitized cells and healthy erythrocytes in two squares; (b) different cultures of parasitized cells



Pharmacokinetic parameters

PK parameters were calculated by the non-compartmental method from the plasma concentration-time data. The area under the curve (AUC) from zero time to the last observed time [AUC (3 hrs)] was calculated by the linear trapezoidal rule for ascending data points. The area obtained by extrapolating from the last point to infinity [AUC(3 hrs-∞)] was calculated by dividing the estimated concentration at the last data point with the elimination rate constant which was estimated by log-linear regression of the terminal 3, 4 or 5 plasma concentration-time data points. The total area under the plasma concentration curve was calculated as $AUC(\infty) = AUC(3 \text{ hrs}) + AUC(3 \text{ hrs}-\infty)$. The maximum plasma concentration (C_{\max}) was obtained directly from the plasma concentration-time data.

In order to illustrate the effectiveness of a cocrystal formulation, two dimensionless parameters of rAUC (ratio of the area under curve of a cocrystal formulation relative to parent

API) and rC_{max} (ratio of the peak concentration of a cocrystal formulation relative to parent API) are given by,

$$rAUC = \frac{AUC(ART\ cocrystal)}{AUC(ART)} \quad (2)$$

$$rC_{max} = \frac{C_{max}(ART\ cocrystal)}{C_{max}(ART)} \quad (3)$$

ART plasma concentration determination by Liquid Chromatography-High Resolution Mass Spectrometry (LC-HRMS)

The samples collected from the mouse plasma were subjected to a protein precipitation extraction process before they were analysed by LC-HRMS machine for ART concentration determination. Samples were taken from -80°C and thawed at room temperature. 10 μL of each plasma sample was mixed with 40 μL of acetonitrile containing 100 ng/mL SAN as the internal standard, and was placed in an Eppendorf micro tube for processing. The mixture was vortexed for 5 min and centrifuged for 20 mins at 10,000 rpm in an Eppendorf 5415R refrigerated centrifuge (Eppendorf Limited, Stevenage, UK) at 4°C . The clear supernatant was filtered with a 4 mm PTFE membrane 0.2 μm syringe filter from Phenomenex (Macclesfield, U.K.) prior to analysis on LC-HRMS.

The LC-HRMS system consisted of an Agilent 1290 UPLC coupled to an Agilent 6530 QTOF mass spectrometer (Agilent Technologies Ltd, Cheshire, UK), operated in the TOF mode with a 20 parts-per-million mass to charge window. The target drugs were analysed on a Kinetex UHPLC C18 column (1.7 μm , 2.1 mm X 100 mm) which was preceded by a security guard ultra-cartridge (Phenomenex, Macclesfield, UK). The column oven temperature was set to 25°C . The mobile phase consisted of water containing 0.3% formic acid (eluent A) and methanol (eluent B) and was delivered in 20:80 v/v respectively at 0.3 mL/min flowrate, with a run time of 3 mins. The sample injection volume was 10 μL .

The mass spectrometer was operated in a positive ion mode with an electrospray ionization source. The chamber conditions were optimized to give maximum analyte signal intensities as follows: Fragmentor voltage: 150V; Gas temperature: 150°C ; Dry gas: 6 l/min; Nebulizer: 30.0

psig; Sheath gas temperature: 350°C; Sheath gas flow: 7.5 l/min; Mass range: 100-1000 m/z; recording rate 4 GHz, HiRes; HRMS lock reference masses: 121.0508 m/z and 922.00987 m/z. Mass Hunter Workstation Acquisition Software for TOF/Q-TOF version B.08.00 (Agilent Technologies Ltd., Cheshire, UK) was used to operate the system and acquire all data. The data was processed using Mass Hunter Workstation Qualitative Analysis Software Version B.07.00 (Agilent Technologies Ltd., Cheshire, UK). An external calibration of the TOF mass spectrometer was performed daily prior to the analysis.

To prepare the calibration standards, 10 µL of 1×10^6 ng/mL ART stock solution prepared in acetonitrile was used to spike 990 µL blank mouse plasma to provide a final ART plasma concentration of 1×10^4 ng/mL. Dilutions with the blank mouse plasma were carried out to provide a series of calibration standards, i.e. 50, 100, 250, 500, 750 and 1000 ng/mL with the validation samples of 350 and 800 ng/mL. 10 µL of each of the standards was mixed with 40 µL of acetonitrile containing 100 ng/mL SAN as the internal standard for protein precipitation extraction as described above. The accurate masses of the target drug ART and internal standard SAN were determined prior to sample analysis. A standard mass spectrum in the full scan range 100-1000 m/z was obtained by injection of 10 µL of each of the supernatants. The most intense ions (m/z species) under the chosen operating conditions were: ART 283.1540 MH⁺; SAN 247.1329 MH⁺. The retention times were 0.9 and 1.1 mins for SAN and ART respectively. ART's LC-HRMS method parameters, detailed calibration curve and validation can be found in Table S4 in the supporting materials.

PBPK Modelling

The Simcyp mouse simulator (Version 19 Release 1, SimCYP®, Sheffield, UK) is employed to simulate the ART plasma concentration-time profiles of a formulation in the systemic circulation of a mouse after dosing on D1 or D4. The *in silico* PBPK mouse model within the simulator is based on the general anatomy and physiology of a 0.025 kg non-strain specific mouse, which is similar to those used in the tests. Therefore, the default mouse physiology and

anatomy (system) parameters incorporated in the Simcyp mouse simulator were selected in the ART PBPK model. The required relevant physicochemical, physiological and pharmacokinetic input data of ART in the simulations are shown in Table 1, which have been taken from the literature [51-58]. Solid formulation (immediate release) was selected as formulation type in the simulations where *in vitro* dissolution data of the ART formulation obtained in section 2.2.3, which has been converted into % drug dissolved shown in Table S9 in the supporting materials, were used as the inputs to the *in silico* PBPK mouse model. Due to the difference of the dissolution environments, time to achieve the same released percentage of the ART *in vivo* could be significantly different from that in the *in vitro* experiment. To reflect this, a dissolution scalar constant K_{diss} between the sampling times of the *in vitro* dissolution and *in vivo* experiment was introduced (details can be found in Table 1). *In silico* clinical trials were carried out over a time period of 24 hours following a single orally administered dose of 30 mg/kg. All simulations were carried out in fed mice to mimic the *in vivo* studies. In order to achieve the best simulations of the plasma concentration-time profiles and PK parameters [i.e., C_{max} , T_{max} (time to C_{max}), and AUC] of the ART formulation using the PBPK model, a sensitivity analysis was carried out. The adjusted parameters included the dissolution scalar constant K_{diss} , blood to plasma ratio B/P, the tissue to plasma partition coefficient K_p scalar, and the oral clearance (CL_{po}) using the ART plasma concentration-time profile after the first dose on D1. In order to verify the reliability of the developed PBPK model, a simulation was performed to simulate the ART plasma concentration-time profile of the ART alone formulation on D4. All of the parameters in the trial designs of the fourth dose on D4 were same as those of the first dose on D1 except the ART oral clearance due to the auto induction of CYP enzyme in a multiple-day treatment. The studies have shown that the ART oral clearance could increase 3-6 fold over the days in a multiple-day treatment [40-44]. In this study, the oral clearance $CL_{\text{po-D4}}$ of the fourth dose D4 was calculated by Eq. (4) in Table 1, which is inverse to its $AUC_{D4}(\infty)$.

Finally, the predicted plasma concentration-time profiles of ART cocrystal formulations after the first dose D1 and the fourth dose D4 were obtained by the developed PBPK model with the inputs of *in vitro* dissolution data measured in section 2.2.3. Fig. 3 illustrates the strategy for developing the PBPK models to predict the plasma concentration-time profile of an ART cocrystal formulation.

Table 1: Parameters used for ART PBPK modelling simulations in Simcyp Mouse Simulator

Parameter	Initial unoptimized Value	Ref/ comments	Final optimized value
<i>PHYSICOCHEMICAL AND BLOOD BINDING PROPERTIES</i>			
Molecular weight (g/mol)	282.332		
Log P o: w (Logarithm of the Octanol-water partition coefficient)	2.9	[59]	Same as initial value
Compound Type	Neutral		
B/P (Blood to plasma partition ratio)	1.10	The range of B/P value from 1.10 to 1.60 was obtained from a rat <i>in vitro</i> blood distribution study [57]. A sensitivity analysis was run to determine the optimal B/P.	1.27
f _u (Fraction unbound in plasma)	0.14	f _u value was obtained from the literature [58] and it was also validated by the rat plasma [52]	Same as initial value
<i>ABSORPTION RELATED PARAMETERS</i>			
Absorption model	ADAM		
F _u gut	0.14	Assumed same as f _u plasma [60]	Same as initial value

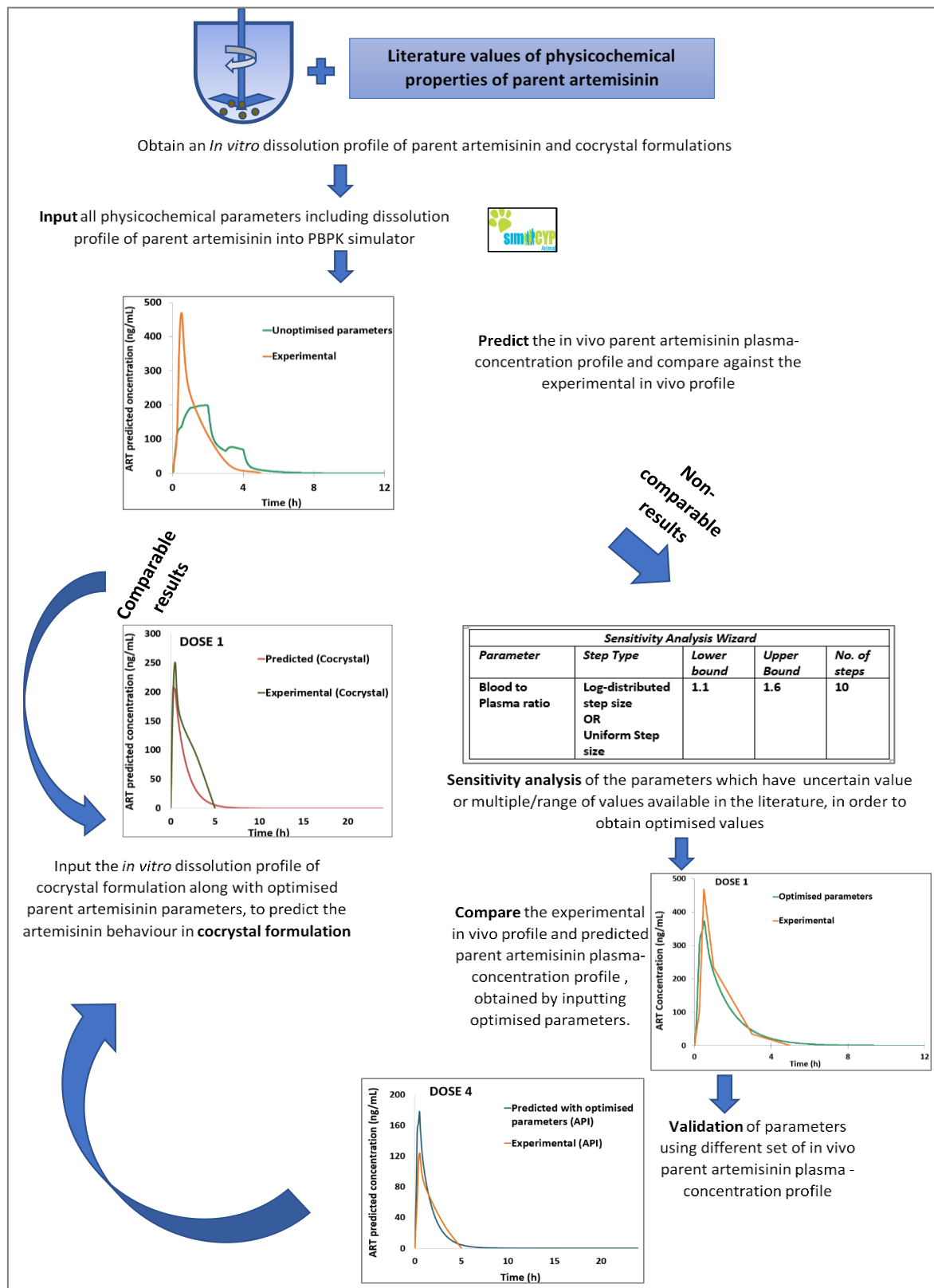
(Fraction of drug unbound in the gut)			
Effective mouse jejunum permeability (P_{eff})	1.44 X 10 ⁻⁴ cm/s	P_{eff} was obtained from an in situ rat perfusion model [43]	Same as initial value
Absorption rate scalar	1	Default value within Simcyp mouse simulator	Same as initial value
Formulation type	Solid formulation; Immediate release; <i>In vitro</i> dissolution profile in pH 6.8 PBS 0.01M (USP II) with pre-dissolved 0.05 mg/mL PVP-VA polymer. Discrete, Fed mode, not allowing non-monotonic dissolution profile.		
Dissolution scalar constant K_{diss} where	No Dissolution scalar used i.e. $K_{diss}=1$.	% of drug dissolved over time was entered in the simulator and calculated as (Table S9) Each dissolution time point was divided by K_{diss} when an <i>in vitro</i> dissolution profile of a formulation was input into the PBPK model. A sensitivity analysis was conducted on K_{diss} values from 0.5-12.	8
<i>DISTRIBUTION PARAMETERS</i>			
Model	Full PBPK model		
V_{ss} (L/kg) (Steady -state volume of distribution)	0.18	K_p scalar was adjusted to obtain V_{ss} in range 0.1-1L/kg from literature value[54, 61].	0.22
K_p scalar (Tissue-plasma partition coefficient)	0.003	A built-in model of Rodgers and Rowland (Method 2) was used.	0.01
<i>ELIMINATION PARAMETERS- In vivo clearance</i>			

CL _{po} (mL/min) (Oral plasma clearance)	CL _{po-D1} =4.40mL/min for first dose D1	CL _{po} in female rats after single ART dose = 10.6 L/(h.kg); weight of mouse in simulation= 0.025 kg. Therefore CL _{po} = 4.40 mL/min [52]	CL _{po-D1} = 3.53 mL/min for first dose D1
	CL _{po-D4} = 11.57 mL/min for fourth dose D4	The ART oral clearance correction due to auto induction of CYP enzyme in a multiple-day treatment $CL_{po-D4} = \frac{CL_{po-D1}AUC_{D1}(\infty)}{AUC_{D4}(\infty)}$ (4)	CL _{po-D4} = 9.28 mL/min for the fourth dose D4

TRIAL DESIGN

Duration of study (hours)	24	Same as planned experimental <i>in vivo</i> study
Fluid intake with dose (mL)	0.20	
Dosing (mg/kg)	30	
Substrate	Oral, single dose, fed state	

Fig.3: Strategy of development of the PBPK models to predict the plasma concentration-time profile of an ART cocrystal formulation



Results

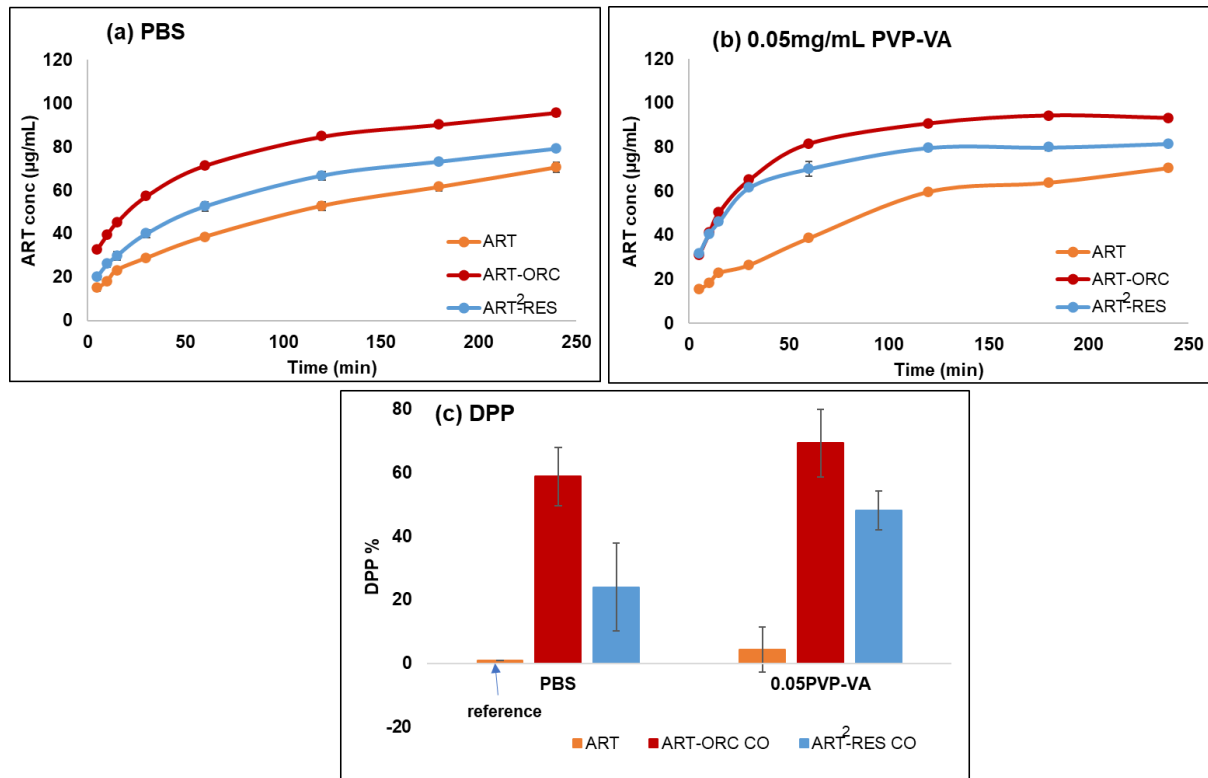
In vitro dissolution tests

In the first part of our study on formulation development, it was shown that PVP-VA at 0.05 mg/mL concentration was the optimal value for *in vitro* dissolution/permeation study [36]. In this study, the dissolution performance parameter (DPP) was used for evaluating the dissolution profile of ART cocrystals in the absence or presence of pre-dissolved PVP-VA polymer in comparison to a reference system of ART in PBS [12]. DPP allows a quantitative comparison of the dissolution performance of a cocrystal formulation with the parent drug formulation, where a positive DPP value indicates an increased ability to dissolve and to be maintained in a dissolution medium whereas a negative DPP value indicates that the formulation has a less ability to dissolve and to be maintained in solution [12].

Fig. 4 shows the dissolution profiles of ART, ART-ORC and ART²-RES in the absence and presence of 0.05 mg/mL of PVP-VA, under non-sink conditions. In the presence of the polymer, ART solids showed a dissolution profile very similar to the one without the polymer and its DPP value was 4% higher when the dissolution profile of ART in PBS was selected as the reference.

ART-ORC and ART²-RES showed an advantage of improved dissolution relative to ART solids both in the presence or absence of a pre-dissolved 0.05 mg/mL PVP-VA polymer. In case of ART-ORC, the presence of PVP-VA showed an increase of DPP to 69% from 58% in PBS alone. In the case of ART²-RES, PVP-VA polymer shows an increased DPP of 48% as compared to 26% in pure PBS alone. These results are very similar to powder dissolution studies in presence 0.1 mg/mL PVP-VA concentration (as shown in Part 1 of the study [36]), however, as described in that paper, the 0.05 mg/mL PVP-VA is the most optimal concentration for both dissolution/permeation study.

Fig 4: Comparison of *in vitro* dissolution profiles of different formulations in the absence and presence of 0.05 mg/mL of PVP-VA (a) comparison of *in vitro* dissolution profiles of ART, ART-ORC and ART²-RES in PBS; (b) comparison of *in vitro* dissolution profiles of ART, ART-ORC and ART²-RES in PBS in the presence of 0.05 mg/mL of PVP-VA; (c) comparison of DPPs of different formulations.



Stage 1: treatment regimens at a fixed ART dose of 30 mg/kg

Fig. 5 shows the representative images of smeared blood thin films taken from different groups of mice over the period of D2 to D5. The blood smears contained both healthy erythrocytes and parasitized cells. There was a mixed culture of parasitized cells observed in the blood smears from the infected mice including merozoite invasion of erythrocytes, ring stage, trophozoite and schizont formation (containing merozoites), rupture (releasing merozoites) and gametocytes [50].

The results show that the parasitized cells in all groups represent either the merozoite invasion of erythrocytes (green arrow in Fig. 5) or ring stage (orange arrow in Fig. 5) of the malarial infection on D2 (at 24 hrs post-infection) of the Stage 1 experiments, indicating the effectiveness of the infection process in the experiments. The percentage of healthy erythrocytes (blue arrow in Fig. 5) is significantly higher than the parasitized cells in all groups of mice.

On D3 of the experiments, an increase in parasitized cells in G1 with untreated mice and G3 with ART treated mice is observed where mostly ring stages and some trophozoites are observed (red arrow in Fig.5). In G4 and G5 treated by ART cocystal formulations on D3, the parasitized cells at ring stage and some trophozoites were also observed. However, there is no significant increase of the number of parasitized cells in G4 or G5. Overall, the number of healthy erythrocytes is still higher than the parasitized cells in all groups on D3.

On D4, the parasitized cells of mice in G1 and G3 show presence of ring stage, trophozoite and formation of schizont (yellow arrow in Fig.5) as well as a few ruptured schizont (black arrow in Fig. 5) and gametocytes (pink arrow in Fig. 5). The number of healthy erythrocytes reduced significantly as compared to previous days of the infection in both groups. In the meantime, it is clearly shown that the number of the infected cells in G3 is much lower than that in G1 in Fig. 5, indicating the effectiveness of ART treatment against *Plasmodium berghei* infection. On the same day, parasitized cells were observed in the G4 and G5 sample, including ring stage, trophozoite, formation of schizont as well as a few ruptured schizonts and gametocytes. However, the number of parasitized cells is significantly lower as compared to those of ART treatment in G3, indicating the improved efficacy of the ART cocystal formulation treatments.

On D5, the sample slides in G1 and G3 are largely covered by the parasitized cells, presenting ring stage, trophozoite and formation of schizont as well as a multiple ruptured schizonts and

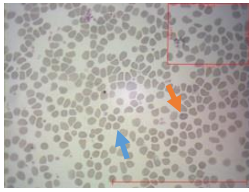
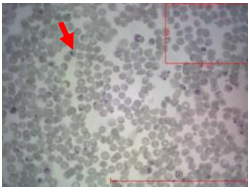
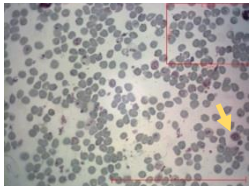
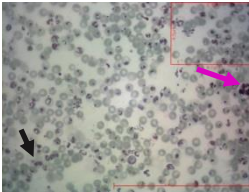
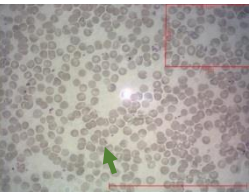
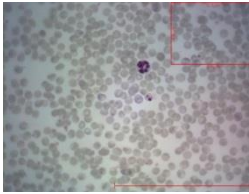
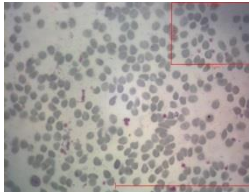
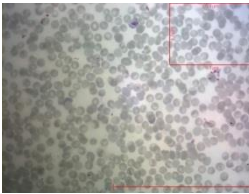
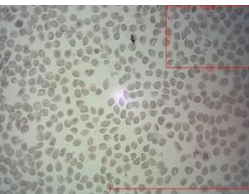
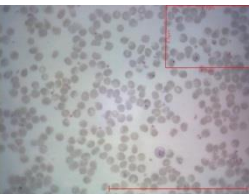
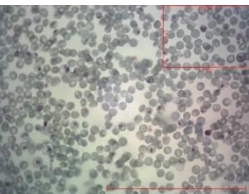
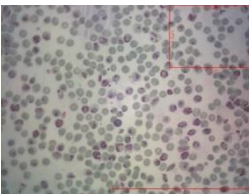
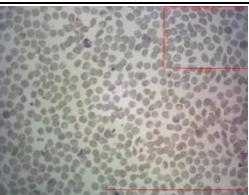

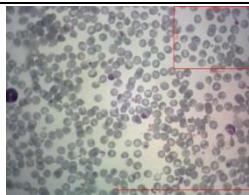
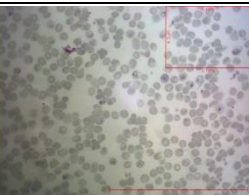
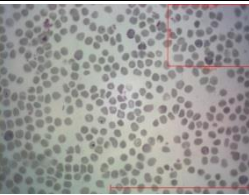
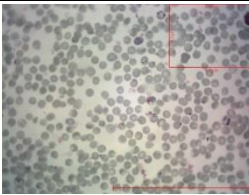
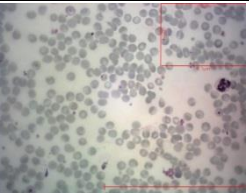
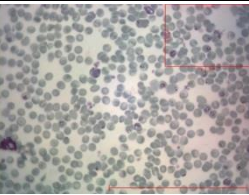
gametocytes. The rupturing of schizont is confirmed by presence of free merozoites in the bloodstream which were also stained on the slides. In contrast, the number of parasitized cells on the sample slides of G4 and G5 has no increase, which is significantly lower than that in G3 or G1.

It is worth noting that the two ART cocrystal formulations (i.e., ART-ORC and ART²-RES) show similar effectiveness against *Plasmodium berghei* infection, as indicated by a similar number of the parasitized cells in G4 and G5 from D2 and D5. For the mice in G2 treated with 10 mg/kg CQ the number of parasitized cells on the slides was extremely low compared to the healthy erythrocytes and no significant increase of the number of parasitized cells was observed from D2 to D5, supporting the evidence that chloroquine is the most effective drug for treatment of *Plasmodium berghei* infection [47].

The quantitative comparison of the percentage parasitaemia of *Plasmodium berghei* under different treatments is shown in Fig. 6(a) (the data are given in Table S5 in the supporting materials). For the untreated mice in G1 the percentage parasitaemia of *Plasmodium berghei* in blood increased significantly over the five-day period, starting from 2.2% on D2 to 58% on D5, indicating the *Plasmodium berghei* grew rapidly in the mouse blood circulation. Under the treatment of CQ in G2, the infected blood cells of the mice were very low, with 2% parasitaemia over the five-day period. The percentage parasitaemia of the mice in G3, treated with 30 mg/kg ART, showed a considerably increasing trend, starting from 1.4% on D2 to 32% on D5, although it is lower compared to that of control G1 (58%) with no treatment. The mice in G4 and G5 were treated with ART cocrystal formulations, i.e., ART-ORC and ART²-RES respectively, where the ART dose of 30 mg/kg was used as same as that of ART alone in G3. Two ART cocrystal formulations achieved the same percentage parasitaemia, i.e., ~6%, which was significantly lower than that of the mice in G3 treated with ART alone.

The ART plasma concentration-time profiles, i.e., dosing regimen 1 which was the first dose given on D1 after the mice were infected and dosing regimen 2 which was the fourth dose given on D4, are shown in Fig 7(a). In the dosing regimen 1, all of the formulations generated the highest ART concentrations at 0.5 hr, i.e., 572 ± 311 ng/mL in G3, 941 ± 19 ng/mL in G4 and 783 ± 157 ng/mL in G5. A complete elimination was observed after 3h of dosing the ART alone formulation in G3. In contrast, ART can be detected in the blood at 3 hrs for both cocrystal formulations in G4 and G5, 153 ± 91 ng/mL and 160 ± 0 ng/mL respectively. Overall, the performance of the ART-ORC formulation was slightly better than that of ART²-RES formulation. The relative ART exposures (rAUC) of the cocrystal formulations to the ART alone formulation are 2.28 for ART-ORC and 2.22 for ART²-RES. The ART plasma concentration-time profiles in the dosing regimen 2 after the repeated dose on D4 (Fig. 7a) show the same trend as those in the dosing regimen 1. There was no obvious difference of the ART concentration-time profiles of the two cocrystal formulations, which are significantly higher than that of ART alone formulation. The relative ART exposures to the ART alone formulation are 2.59 for ART-ORC formulation and 2.55 for ART²-RES formulation. The maximum ART concentrations were also generated at 0.5h, treated with the ART cocrystal formulations, i.e., 246 ± 33 ng/mL in G4 and 239 ± 6 ng/mL in G5. A complete elimination was observed after 3h of dosing ART alone formulation in G3. Similarly, ART was detected at 3 h for both cocrystal formulations, which was 75 ± 2 ng/mL treated with ART-ORC formulation in G4 and 60 ± 1 ng/mL treated with ART²-RES formulation in G5. It has to be stressed that the maximum concentrations and exposure of ARTs in the dosing regimen 2 were significantly reduced by more than 2-fold than those in the dosing regimen 1 for all of formulations. A summary of results is shown in Table 2.

Fig. 5: Representative images of smeared blood samples from experiment (i)

Group no. /treatment	D2	D3	D4	D5
	mean±SD	mean±SD	mean±SD	mean±SD
Group 1-untreated	2.2±0.4	7.4±0.9	14.5±2.5	58.5±4.7
				
Group 2-10 mg/kg CQ	2.5±0.3	2.1±0.6	1.4±0.1	2.7±0.4
				
Group 3-30 mg/kg ART	1.5±0.2	5.8±0.4	8.4±0.6	33.0±1.1
				
Group 4-30 mg/kg ART-ORC	1.5±0.2	3.8±0.3	4.6±0.2	6.5±1.3
				
Group 5-30 mg/kg ART ² -RES	1.5±0.1	4.1±0.3	5.5±1.3	6.3±1.7
				








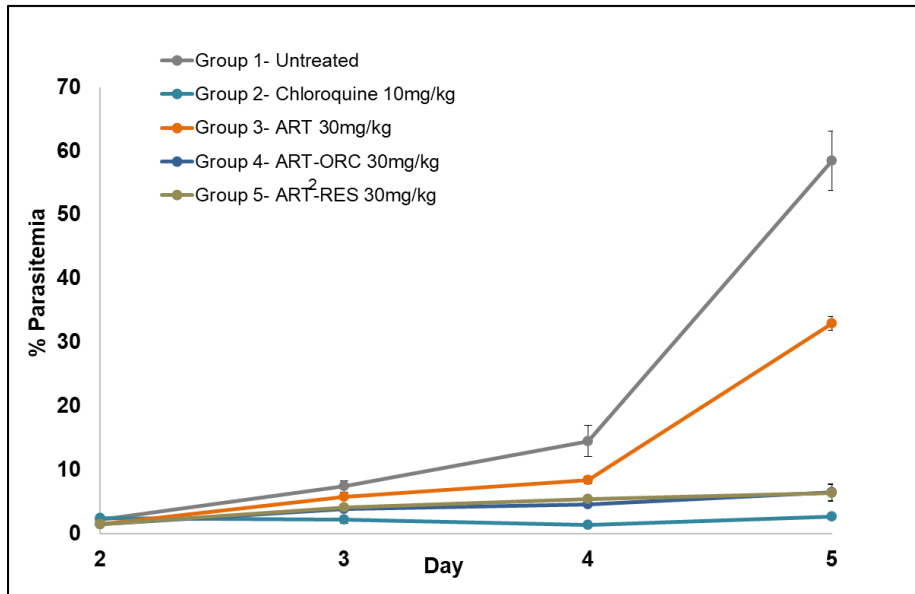
Note: : healthy erythrocytes; : the merozoite invasion of erythrocytes; : ring stage of the malarial infection; : trophozoites; : formation of schizont; : ruptured schizont; : gametocytes

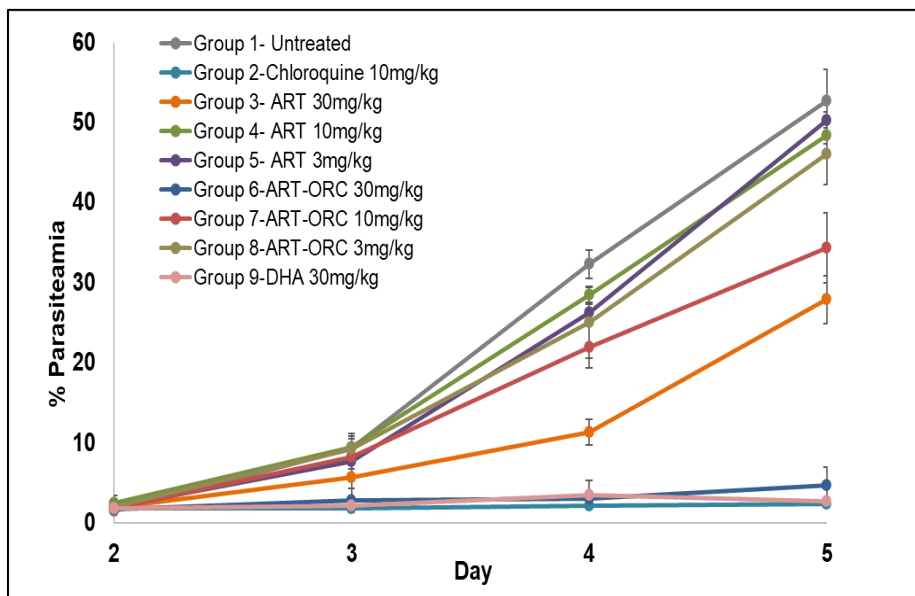
Table 2: PK parameters of the experiments (i) and (ii)

Regimen 1							Regimen 2				
	Formulation	C _{max} (ng/mL)	T _{max} (h)	AUC (ng/mL*h)	rAUC	rCmax	Cmax (ng/mL)	Tmax (h)	AUC (ng/mL*h)	rAUC	rCmax
Stage 1	ART	572	0.50	369	1.00	1.00	91	1	165	1.00	1.00
	ART-ORC	941	0.50	840	2.28	1.64	246	0.50	426	2.59	2.70
	ART ² -RES	783	0.50	818	2.22	1.37	239	0.50	420	2.55	2.61
Stage 2	ART	363	0.50	685	1.00	1.00	164	0.50	236	1.00	1.00
	ART-ORC	1098	0.50	1440	2.10	3.02	256	0.50	430	1.82	1.56
Avg of Stage 1 and 2	ART	468	0.50	527	1.00	1.00	123	0.50	200	1.00	1.00
	ART-ORC	1019	0.50	1140	2.16	2.18	251	0.50	428	2.14	2.04

Fig. 6: comparison of percentage parasitaemia under different treatments (a) at a fixed ART dose in Stage 1; (b) at various fixed ART doses in Stage 2.

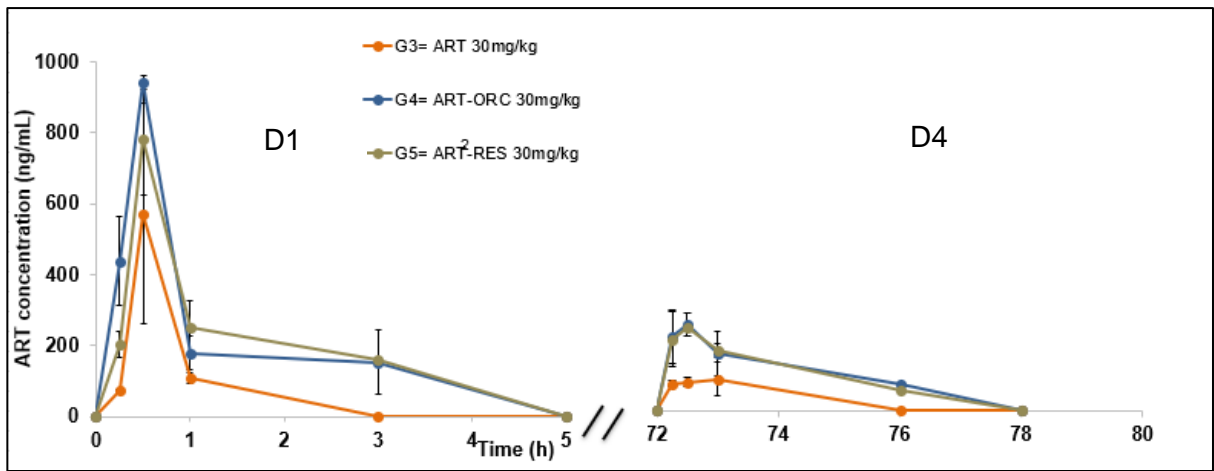


(a)

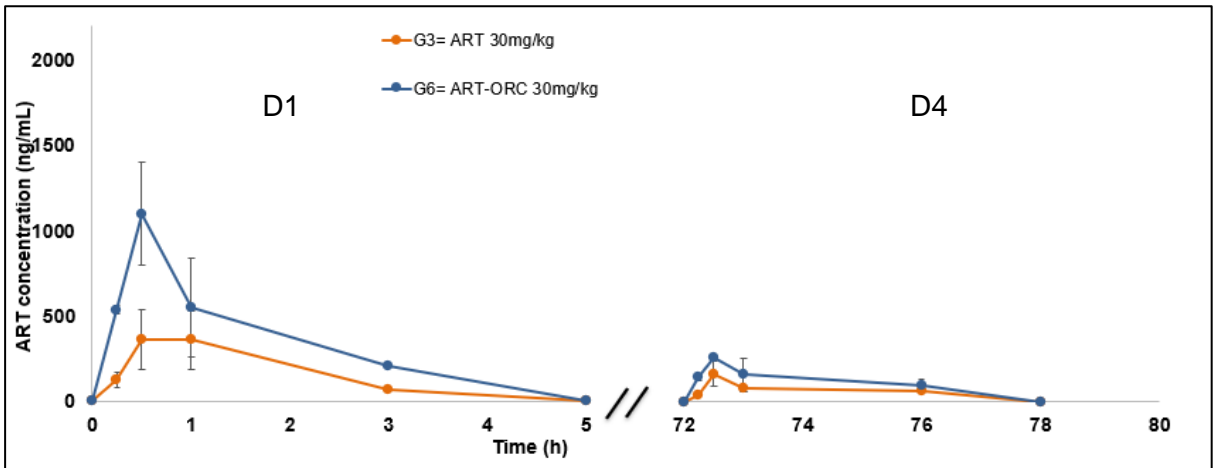


(b)

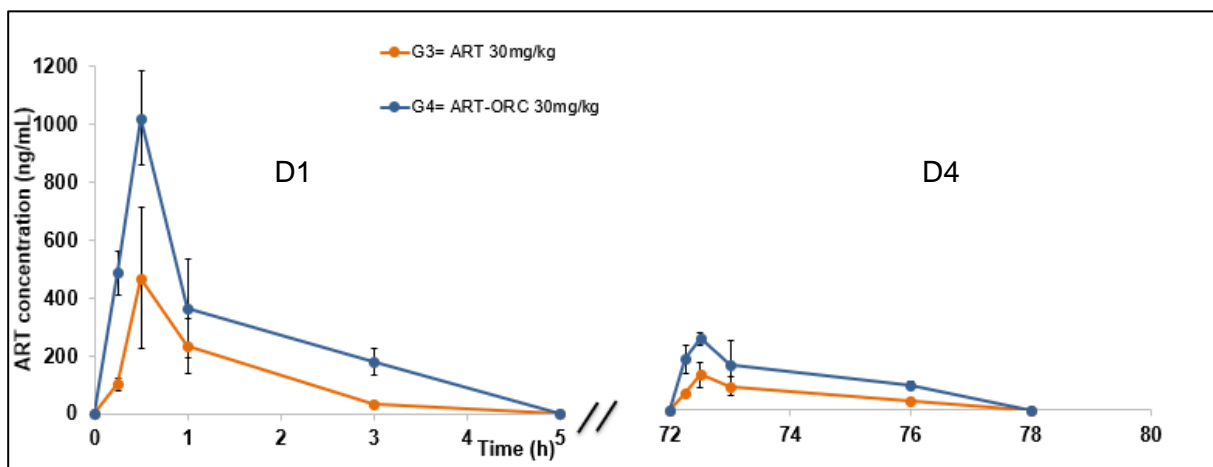
Fig. 7: ART concentration-time profiles at a fixed dose of ART 30 mg/kg (a) Stage 1; (b) Stage 2; (c) Average Stage 1 and Stage 2



(a) Stage 1



(b) Stage 2



(c) Average of Stage 1 and Stage 2

Stage 2: Dose response treatment regimes

The best performing ART cocrystal formulation, ART-ORC, was selected for the second Stage tests, aiming to establish repeatability and to determine any dose-response effect of the ART cocrystal formulation. The various ART doses of 3 mg/kg, 10 mg/kg and 30 mg/kg for both ART-ORC and ART alone formulations were conducted in the test. The references of the experiments included the untreated mice in G1 and those treated by CQ solution at a dose of 10 mg/kg in G2. Dihydroartemisinin (DHA), which is a derivative of ART and a well-known artemisinin derivative used in ACT, was also tested at a dose of 30 mg/kg in the Stage 2 experiments and parasitaemia percentage was calculated for this group.

The evolution of the percentage parasitaemia of *Plasmodium berghei* under different treatments is shown in Fig. 6(b) and data is given in Table S6 in the supporting materials. The percentage parasitaemia of *Plasmodium berghei* of the untreated mice in G1 increased significantly over the five-day period, from 1.5% on D2 to 52% on D5. Treated with 10 mg/kg CQ in G2 and 30 mg/kg DHA in G9, the infected cells of the mice remained as low as ~2% over the same period. The mice in G3, G4 and G5 were treated by ART alone formulation with various dose strengths of 30 mg/kg, 10 mg/kg and 3 mg/kg respectively. It was observed that the percentage parasitaemia of mice in G3 treated by 30 mg/kg ART increased from 1.9% on D2 to 27% on D5. With a reduced ART dose, the percentage parasitaemia of *Plasmodium berghei* increased significantly, i.e., from 2% on D2 to 48% under the dose of 10 mg/kg and to 50% under the dose of 3 mg/kg on D5, respectively. They were almost the same as those of untreated mice in G1. The mice in G6, G7 and G8 were treated by the ART-ORC formulation with the various ART dose strengths of 30 mg/kg, 10 mg/kg and 3 mg/kg respectively. The percentage parasitaemia of mice in G6, which were treated by 30 mg/kg ART of ART-ORC formulation, slightly increased from 1.7% on D2 to 4.6% on D5. The percentage parasitaemia of mice in G7 and G8, which were given 10 mg/kg and 3 mg/kg ART of the ART-ORC

formulations, increased from 1.8% on D2 to 34% on D5 and from 2% on D2 to 46% on D5 respectively.

The ART plasma concentration-time profiles were also obtained for the treatments of ART-ORC and ART alone formulations at an ART dose strength of 30 mg/kg, aiming to investigate the repeatability of the results. The ART plasma concentration-time profiles of both the dosing regimen 1 (D1) and dosing regimen 2 (D4) are shown in Fig 7(b). The summary of the PK parameters is shown in Table 2. Although there were variations of ART concentrations at the sampling points, the trends of the ART plasma concentration-time profiles are same, i.e., ART concentration-time profile of ART-ORC formulation is much higher than that of ART alone formulation and significant reductions of the maximum concentrations and exposure of ARTs in the dosing regimen 2 were also observed. In particular, the two dimensionless parameters of $rAUC$ and rC_{max} in both of the dosing regimens of the two-Stage tests are comparable, showing a good repeatability of the experiments.

PBPK modelling

Due to the pharmacokinetic variability within the mouse populations, the averaged ART plasma concentration profile of the dose regimen 1 on D1 obtained from both Stage 1 and Stage 2 tests shown in Fig 7(c) was used for the PBPK model development while that of the dose regimen 2 on D4 was used for the model validation.

Simulations of the oral mouse plasma concentration-time profiles for the ART alone formulation were performed, with the model inputs including the *in vitro* dissolution data in Fig. 4(b) and the drug specific properties (initial unoptimized value) in Table 1. Because of the difference of the dissolution environments, dissolution times reaching the same percentages of the dissolved ART in the formulation between *in vitro* and *in vivo* could be significantly different. Consequently, a large discrepancy between the predicted and measured ART concentration-time profiles can be observed if the *in vitro* dissolution data [Fig. 4(b)] were used

directly as inputs to the model along with unoptimized values (Table 1), as shown in Fig. 8(a). The C_{max} was off by 2.35-fold and T_{max} was higher by almost 3.76 times and AUC was approximately the same, detailed in Table S7 in the supporting materials. The shape of concentration vs time profile was very different as compared to the experimental profile. Additionally, the predicted oral mouse plasma concentration-time profile was highly dependent on the ART specific properties in Table 1. Most of the parameters obtained are consistent from different sources while the others show a big discrepancy, in particular B/P with a range from 1.10 to 1.60 [57] and V_{ss} with a range from 0.1 to 1 L/kg [54]. In order to achieve these values of V_{ss} in the simulations, K_p scalar value has to be adjusted accordingly from 0.003- 0.200 in the Simcyp settings, which is a requirement of a full PBPK model.

As the first step of the oral PBPK model development, parameter sensitivity analysis was used to investigate the impact of the changes of the dissolution scalar constant K_{diss} , blood to plasma partition ratio B/P and tissue-plasma partition coefficient K_p on the oral exposure. The ranges and steps of these parameters investigated are shown in Table S8 in the supporting materials. In these analyses, a constant oral clearance value of 4.40 mL/min in Table 1 was used as found from the literature [52]. A predicted error considering all three key PK measures, i.e., T_{max} , C_{max} and AUC, was calculated as

$$E \left(K_p, \frac{B}{P}, K_d \right) = \frac{1}{r_{Tmax} + r_{Cmax} + r_{AUC}} \left(r_{Tmax} \frac{abs(T_{max_predicted} - T_{max_experimental})}{T_{max_experimental}} + r_{Cmax} \frac{abs(C_{max_predicted} - C_{max_experimental})}{C_{max_experimental}} + r_{AUC} \frac{abs(AUC_{predicted} - AUC_{experimental})}{AUC_{experimental}} \right) \quad (5)$$

where $T_{max_predicted}$, $C_{max_predicted}$ and $AUC_{predicted}$ are the predicted values; $T_{max_experimental}$, $C_{max_experimental}$ and $AUC_{experimental}$ are the experimental values of the averaged ART plasma

concentration profile of the dose regimen 1 (D1) in Stage 1 and 2; $r_{T_{max}}$, $r_{C_{max}}$ and r_{AUC} are the weighting factors.

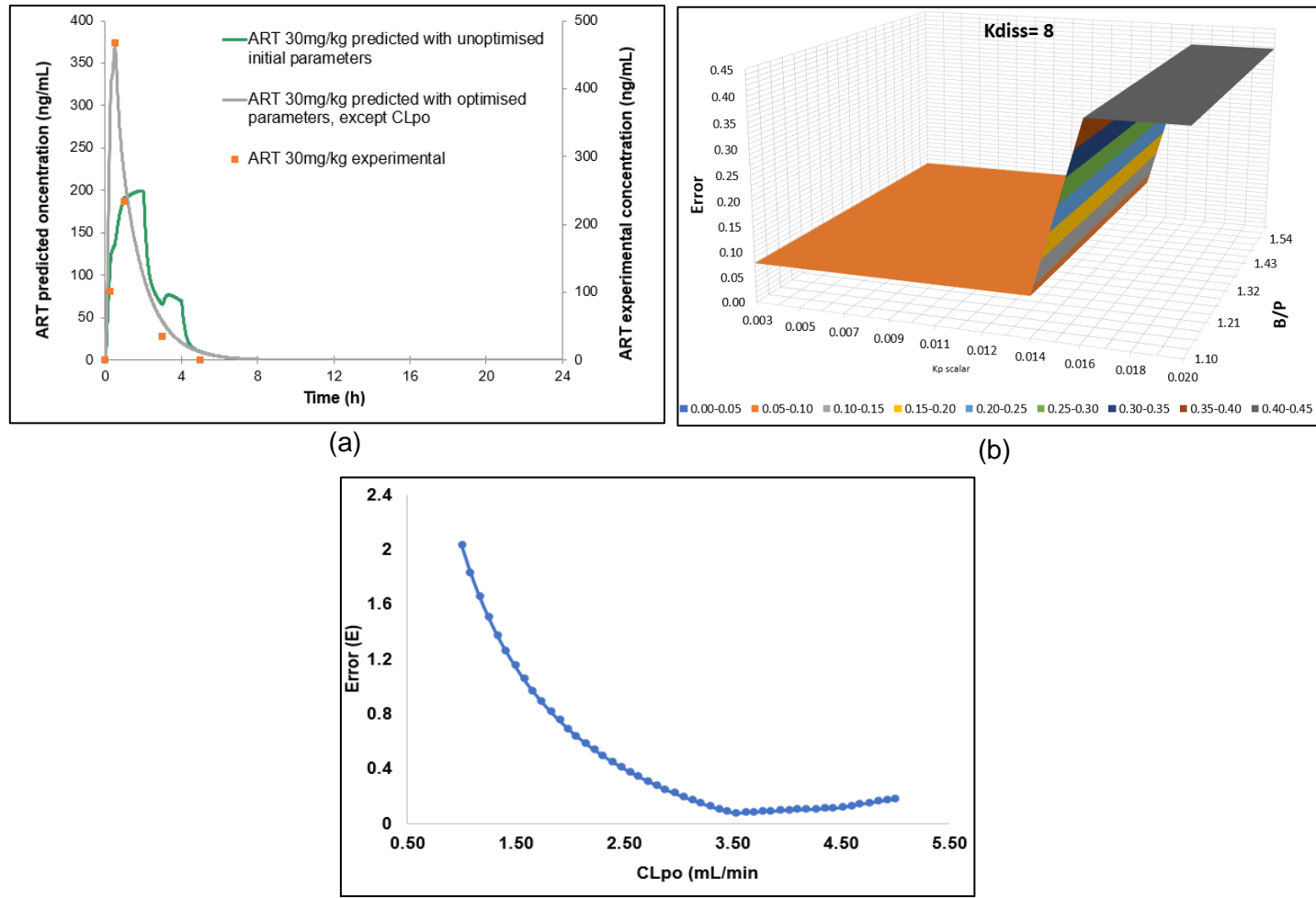
The combinations of the values of K_{diss} , B/P and K_p can result in prediction error within the range of 0.08 - 1.20 (Fig. 8(b) and Fig. S1 in the supporting materials) under the same weighting factors as $r_{T_{max}} = r_{C_{max}} = r_{AUC} = 1$. Initially, the K_p range was selected between 0.003 and 0.200, which showed that the smallest error lay between 0.003-0.020. Therefore, this range was selected to obtain a precise error prediction. The smallest error of 0.08 was obtained by the optimal combination of $K_{diss} = 8$, $K_p = 0.01$ (i.e. $V_{SS} = 0.22$ L/kg) and B/P = 1.27 as shown in Fig. 8(b), under which the comparison of the predicted and experimental ART plasma concentration-time profiles is shown in Fig. 8(a). In comparison with the observed PK values, the C_{max} was off by 1.26-fold and both T_{max} and AUC were the same as experimental values, detailed in Table S7 in the supporting materials.

In order to further improve the accuracy of the model prediction, in particular the prediction of C_{max} , sensitivity analysis of the ART oral clearance CL_{po} within the range of 1-5 mL/min was also conducted under the optimal parameter combinations of K_{diss} , B/P and K_p obtained above. The weighting factors in the prediction error in Eq., (5) were set as $r_{C_{max}} = 2$ and $r_{T_{max}} = r_{AUC} = 1$. The prediction error as a function of the ART oral clearance is shown in Fig 8(c), in which the minimal prediction error was achieved at the oral clearance of 3.53 mL/min. The comparison of the predicted and experimental ART plasma concentration-time profiles with final optimised parameters is also shown in Fig. 9(a) and the detailed PK value comparison is shown in Table 3, indicating the C_{max} , AUC and T_{max} of the ART formulation can be predicted accurately.

The reliability of the developed PBPK model was validated by performing a simulation to predict the ART plasma concentration-time profile of the dose regimen 2 of the ART alone formulation on D4. Because ART induces its own metabolic elimination on repeated doses, a

new *in vivo* oral clearance of 9.28 mL/min was used in the simulation, which was based on the measured *in vivo* data calculated by Eq. (4), while the other parameters were same. Fig. 9(b) shows the comparison of the predicted and measured concentration-time profile and comparison of the predicted and measured PK parameters are given in Table 3. It is shown that the ratios of measured and predicted C_{\max} and AUC for ART were 0.69 and 0.79 respectively. The predicted T_{\max} was exactly the same as the experimental value i.e. 0.5h.

Fig. 8: ART PBPK model development: (a) Comparison of experimental and predicted ART concentration vs time profiles; (b) the predicted error as a function of B/P and K_p with the fixed $K_{diss}=8$ and $CL_{po} = 4.4$ mL/min at the same weighting factors of $r_{Tmax} = r_{Cmax} = r_{AUC} = 1$; (c) the predicted error as a function of the oral clearance CL_{po} with the optimized values of $K_{diss}=8$, B/P=1.27, and $K_p = 0.01$ and the weighting factors of $r_{Cmax} = 2$ and $r_{Tmax} = r_{AUC} = 1$



The ART PK profiles after oral administration of ART cocrystal formulations on D1 and D4 were simulated by the developed mouse PBPK model along with their respective *in vitro* dissolution data [Fig.4(b) and Table S9] as model inputs. Fig. 9 (c, d, e, f) depicts the simulated and observed ART plasma concentration-time profiles of cocrystal formulations and PK parameters are shown in Table 3. It is clearly shown that there is good agreement between observed and PBPK model predicted ART concentrations for both ART cocrystal formulations. The predicted AUCs of the ART cocrystal formulations on D1 and D4 are within 1.5-fold of the observed values, i.e., 1.29 and 1.28 for ART-ORC formulation and 1.06 and 1.43 for ART²-RES formulation. The predicted C_{max} values of the ART cocrystal formulations on D1 and D4 are within 2-fold of the observed values. The predicted T_{max} values of the ART cocrystal formulations, i.e., 0.35 h at D1 dosing and 0.31 at D4 dosing, were lower than those of the observed 0.5 h, which was also expected due to the limited number of observed points in the animal experiments.

Fig. 9: Comparison of predicted and measured plasma concentration-time profiles: (a) ART formulation at D1; (b) ART formulation at D4; (c) ART-ORC formulation at D1; (d) ART-ORC formulation at D4; (e) ART²-RES formulation at D1; (f) ART²-RES formulation at D4

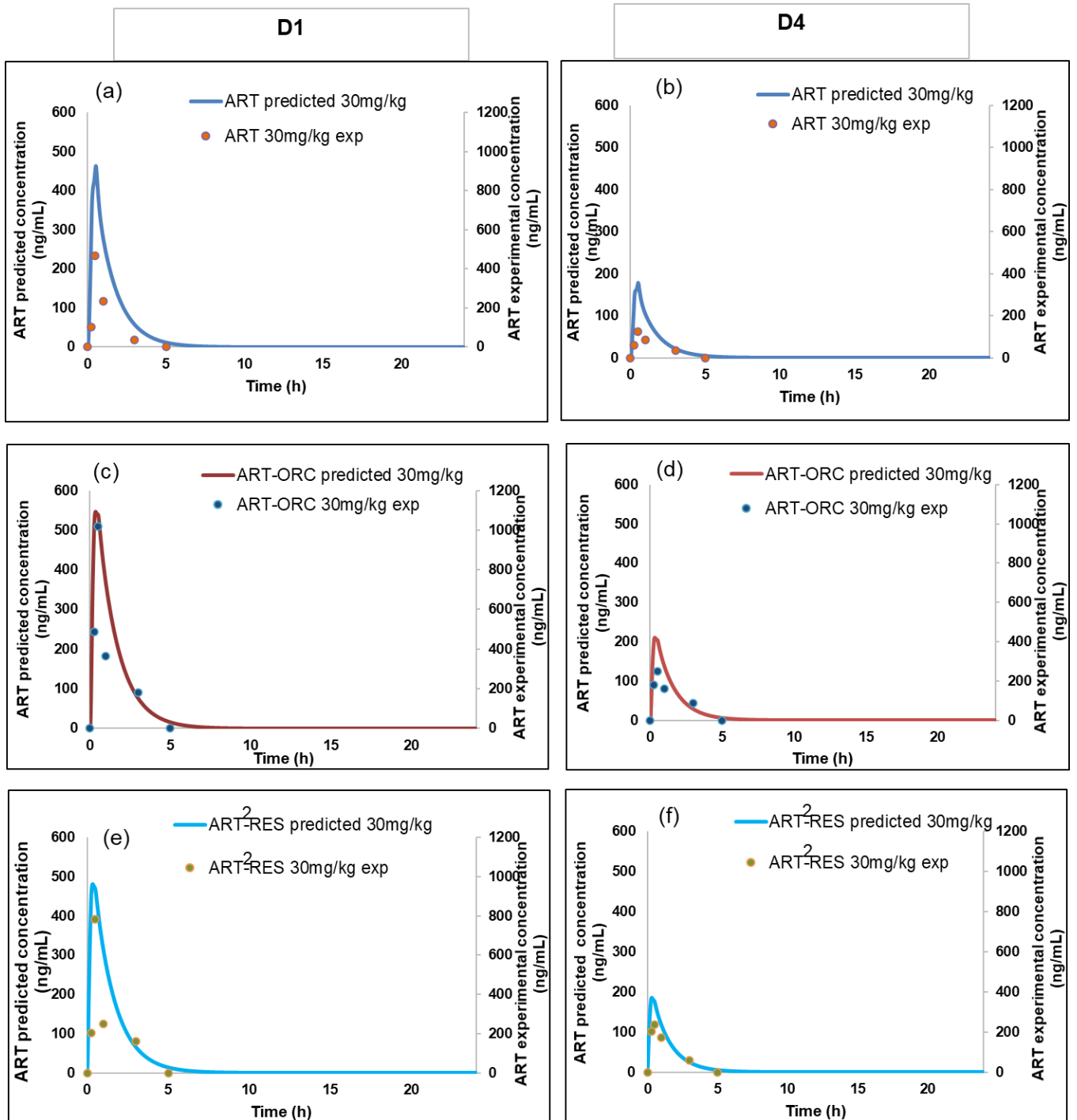


Table 3: Comparison of predicted and measured PK values

	Regimen 1 (D1)			Regimen 2 (D4)		
	C_{max} (ng/mL)	AUC (ng/mL*h)	T_{max} (h)	C_{max} (ng/mL)	AUC (ng/mL*h)	T_{max} (h)
ART						
Experimental	468	527	0.50	123	200	0.50
Predicted	463	666	0.52	178	254	0.50
Ratio	1.01	0.79	-	0.69	0.79	-
ART-ORC						
Experimental	1019	1140	0.50	251	428	0.50
Predicted	546	882	0.35	211	335	0.31
Ratio	1.87	1.29	-	1.19	1.28	-
ART²-RES						
Experimental	783	818	0.50	239	420	0.50
Predicted	482	772	0.35	186	294	0.31
Ratio	1.63	1.06	-	1.28	1.43	-

Discussion and conclusion

Artemisinin-based combination therapies are currently the frontline antimalarial therapeutic agents in clinical use. However, the parent compound ART, cannot be used directly in the therapies because of its extremely low bioavailability caused by its poor water solubility and dissolution rate. The derivatives, such as artemether, arteether, dihydroartemisinin and artesunate, are used in the therapies [62]. However, the production of these semisynthetic derivatives of ART add significantly high manufacturing costs. For example, the cost of ART is around 180–420 US\$/kg in comparison with 3500 US\$/kg of dihydroartemisinin which is used to synthesize other derivatives such as artemether and artesunate. Such high cost has severely restricted their use in many countries where malaria is rife [63].

The work has demonstrated for the first time that cocrystallisation of ART can enhance its clinical performance. In the *in vivo* mouse model study, it has been shown that 58% of the blood cells were infected without treatment after 5 days of infection by *Plasmodium berghei* strains. It is not surprising that the ineffectiveness of clinical outcome was observed when the mice were treated by 30 mg/kg ART formulation, in which 32% of the blood cells were infected on the fifth day. The two ART cocrystal formulations show an outstanding performance against infection of *Plasmodium berghei* in mice. Over the course of the 4-day treatments at a repeated dose of 30 mg/kg, the percentage parasitaemia was kept at 6%, which is a five-fold reduction compared with the treatment by the same dose of ART formulation. The performance of the ART cocrystal formulations was slightly less effective than treatment with chloroquine or dihydroartemisinin which can keep the cell infection rate at 2%. The improved efficacy of the ART cocrystals was supported by the ART PK parameters shown in Fig.7 and Table 3. For regimen 1, the relative ART cocrystal exposures to the ART formulation, rAUC, are 2.16 (averaged Stage 1 and 2) for ART-ORC formulation and 2.22 (Stage 1) for ART²-RES formulation, and relative ART cocrystal maximal concentrations to the ART alone formulation, rC_{max}, are 2.18 (averaged Stage 1 and 2) for ART-ORC formulation and 1.37 (Stage 1) for ART²-RES formulation. For regimen 2, the relative ART cocrystal exposures to the ART formulation, rAUC, are 2.14 (averaged Stage 1 and 2) for ART-ORC formulation and 2.55 (Stage 1) for ART²-RES formulation, and relative ART cocrystal maximal concentrations to the ART alone formulation, rC_{max}, are 2.04 (averaged Stage 1 and 2) for ART-ORC formulation and 2.61 (Stage 1) for ART²-RES formulation. It is shown in Fig.7 and Table 3 that time to reach the therapeutic level decreased significantly due to an increased ART concentration of the plasma concentration-time curve by an ART cocrystal formulation, leading to improved therapeutic effect.

Both the ART and two ART cocrystal formulations revealed time-dependent pharmacokinetics (Fig. 7). A similar reduction of the ART exposure from the first dose to the fourth dose was observed for each of the formulations, *ca.* 50%. This had been observed in other studies with ART before, and is considered the result of induction of several enzymes in the cytochrome P450 (CYP) family, such as CYP2B6 in humans and CYP2B10 in mice, CYP2A6 and CYP3A4, for elimination of ART before reaching the systemic circulation [40-44].

It is highly likely that there is no therapeutic effect by the fourth dose D4 of the ART formulation because of its C_{\max} of 123 ng/mL (averaged over Stages 1 and 2), leading to incomplete parasite clearance in mice. In contrast, the therapeutic effect of an ART cocrystal formulation was likely to be maintained because a significantly higher C_{\max} was observed by the fourth dose D4, i.e., 251 ng/mL (averaged Stage 1 and 2) for ART-ORC and 239 ng/mL (Stage1) for ART²-RES, showing a significant improved performance against infection of *Plasmodium berghei* in mice in Fig. 6.

The dose response test [Fig. 6(b)] indicated that a significantly lower dose of ART cocrystal in the formulation was needed to achieve a similar antimalarial therapeutic effect as ART formulation, i.e., 10 mg/kg of the ART-ORC vs 30 mg/kg of ART or 3 mg/kg of the ART-ORC vs 10 mg/kg of ART were similar. Therefore, the overall additional manufacturing cost of ART cocrystals was expected to be insignificant. A lower dose of ART cocrystals can also reduce toxicity and increase patient compliance to maximize the benefits of the treatments.

Although the *in vivo* mouse study appeared to be effective, a reliable prediction of the pharmacokinetics of the ART cocrystals in human is needed to proceed into the clinic with the designed formulations. Another important issue is related to deciding upon the rank ordering of ART cocrystals for further testing. Although it is not significant here because only two ART cocrystals are available at this stage, the issue could be critical for other compounds. Cocrystals

have the potential for greater flexibility and diversity in the created forms than salts or hydrates due to their compatibility with non-ionizable APIs and a large range of pharmaceutically acceptable coformers that are potentially available, each of which could lead to different pharmacokinetics in human [64, 65]. Early simulations in preclinical species will play a central role in the development of more predictive methods to establish *in vitro* and *in vivo* correlations for different cocrystals intended to improve the properties and to support clinical candidate selection, contributing to assessment of cocrystal developability.

The study has illustrated that information from classical *in vitro* and *in vivo* experimental investigations of the parent drug of ART formulation can be coupled with PBPK modelling to predict the PK parameters of an ART cocrystal formulation in a much more efficient manner. The rationale of the methodology is based on the fact that cocrystals modulate the parent drug pharmacokinetics through changes of its dissolution rate and solubility due to non-covalent bonds in crystal structures. Thus, cocrystals retain the safety and therapeutic properties of the parent API. This is certainly the case for ART cocrystals, showing improved *in vitro* dissolution rates and *in vivo* performance in the mouse model test.

An *in silico* PBPK model using Simcyp Mouse Simulator was successfully built for the ART cocrystal formulation based on the physicochemical and physiological data of ART, the anatomical and physiological parameters of mice and *in vitro* dissolution data of the ART formulation as inputs to fit the oral PK profile measured after the first dose. Sensitivity analysis were performed as a means to optimize particular model parameters with high uncertainties, i.e., K_{diss} , B/P, K_p and CL_{po} in this work. The model was validated using *in vivo* data obtained from the forth dosing, with the same *in vitro* dissolution data as the model inputs. It should be stressed that when applied to predict the *in vivo* PK profiles of ART formulation on repeated dose treatments, the developed PBPK model also needs a time-dependent oral clearance as a model input because of autoinduction of some of the enzymes involved in ART metabolic

elimination. The oral clearance of the fourth dose was corrected by the ratio of the ART exposure to the first dose. Overall, the developed PBPK model was able to reliably simulate the plasma concentration-time profiles of ART, ART-ORC and ART²-RES formulations. The predicted AUC values and C_{max} values of the ART cocrystal formulations at D1 and D4 dosing are within 2-fold of the observed values [66]. These results indicate that the PBPK models were able to accurately capture the observed PK data for ART formulations.

The *in vivo* absorption trend observed is consistent with that of *in vitro* dissolution performance defined by DPP, i.e., higher DPP of a formulation leads to higher *in vivo* absorption. However, a quantitative correlation of *in vitro* and *in vivo* performance proved to be difficult. For example, although the DPPs are significantly different between the two ART cocrystal formulations, similar *in vivo* performances were observed in Fig. 7. Therefore, the developed PBPK model can serve as a means to provide *in vivo* context to the impact of different cocrystal forms on the *in vivo* performance. This is particularly important for those drugs with narrow therapeutic windows. It is likely that the actual T_{max} for ART cocrystal formulations is lower than 0.50h which was determined experimentally due to the limited sampling points. Therefore, it was not unexpected that the predicted T_{max} values of the cocrystal formulations were lower than the experimental values for both dosing regimens. If the *in vivo* experiments were to be repeated again, additional time points can be included. Determination of an increased oral clearance using Eq. 4 was a reliable method as the predicted and experimental values were much closer for all formulations in dosing regimen 2. The variability between the results also has to be taken into account as an average of experimental ART plasma concentration-time profiles was calculated for ART and ART-ORC. It has been seen that ART-ORC has shown highest differences between predicted and experimental results. The average experimental results of Stage 1 and Stage 2 has shown a higher variation. The effect of this has also been observed in predicted results of ART-ORC.

In addition, comparison of the prediction by the PBPK model and the measured *in vivo* PK data can be used for *in vivo* DDI predictions if the coformer is an active ingredient. *In vivo* DDIs can lead to a large discrepancy between the predicted and measured *in vivo* PK data if the DDIs are not built into the PBPK model. In this study, it was clearly shown that there was no DDI between ART with ORC or RES because the developed PBPK model without considering the DDIs can predict the observed ART PK data accurately.

In conclusion, the results of this study generated a scientific framework that will help formulation scientists to adequately evaluate the performance of pharmaceutical cocrystal formulations by applying an optimized PBPK model in an early stage of drug product development. Currently there are many applications using cocrystallisation strategy to improve the existing drug product performance. The *in vivo* data of these parent drugs are readily available. Therefore, in this study we focused on prediction of the *in vivo* performance of the drug cocrystals based on the *in vitro* dissolution performances of the parent drug and cocrystals. The strategy is given in Fig. 3, where the PBPK model of the parent drug was firstly developed and then it was applied to predict the *in vivo* performance of the cocrystals. In our best knowledge, it is the first study as an alternative approach to allometric scaling to be published to guide this important process studies. This can shorten the time needed for the cocrystal product development process. Considering the overall economic gain and the current simulation of an increasing resistance of malaria parasites to quinoline based anti-malarial drugs, the impact of the work could be significant with a huge potential for the ART cocrystals low cost and high efficacy artemisinin-based combination therapies.

ASSOCIATED CONTENT

Supporting Information

The following files are available free of charge.

Table S1: HPLC methods

Table S2: Concentrations for calibration curve on HPLC

Table S3: Validation of calibration curve (x): units in $\mu\text{g/mL}$; C_r : real concentration of validation sample (theoretical) in $\mu\text{g/mL}$ and C_m : measured concentration of validation sample in $\mu\text{g/mL}$.

Table S4: LC-HRMS method to determine ART plasma concentration.

Table S5: Stage 1: Percentage parasitaemia under different treatments at a fixed dose

Table S6: Stage 2: Percentages of parasitaemia under different treatments at various fixed doses.

Table S7: Comparison of predicted and measured PK values with the PBPK unoptimized initial values as model inputs shown in Table 1 and optimal combination of K_{diss} , B/P and K_p without optimized CL_{po}

Table S8: The ranges and steps of the parameters investigated in the parameter sensitivity analysis

Table S9: The *in vitro* dissolution data entered into Simcyp.

Fig S1: Error plots for SA of B/P, K_p and K_{diss}

Corresponding Author

Mingzhong Li* – Tel: +44-1162577132; E-mail: mli@dmu.ac.uk; ORCID: 0000-0002-9532-9049; Leicester School of Pharmacy, De Montfort University, Leicester LE1 9BH, U.K.

Authors

Manreet Kaur – Leicester School of Pharmacy, De Montfort University, Leicester LE1 9BH, U.K.

Vanessa Yardley – Department of Infection & Immunity, Faculty of Infectious & Tropical Diseases, London School of Hygiene and Tropical Medicine, London, WC1E 7HT, U.K.

Ke Wang – Leicester School of Pharmacy, De Montfort University, Leicester LE1 9BH, U.K.

Jinit Masania – Leicester School of Pharmacy, De Montfort University, Leicester LE1 9BH, U.K.

Randolph RJ Arroo – Leicester School of Pharmacy, De Montfort University, Leicester LE1 9BH, U.K.

David B Turner – Certara UK Limited, Simcyp Division, Sheffield, S1 2BJ, U.K.

ACKNOWLEDGEMENTS

We would like to thank the financial support of the work by UK Engineering and Physical Sciences Research Council (EPSRC, EP/R021198/1). The authors also acknowledge Simcyp Limited., a Certara Company, for providing a free academic license of the Simcyp Population-based Simulator and support to conduct the PBPK model development.

All animal work was carried out under a UK Home Office project license according to the Animal (Scientific Procedures) Act 1986 and the new European Directive 2010/63/EU. The project license (70/8427) was reviewed by the London School of Hygiene and Tropical Medicine (LSHTM) Animal Welfare and Ethical Review Board prior to submission and consequent approval by the UK Home Office.

Declarations of interest: The authors declare no competing financial interest.

References

1. Shan, N., et al., *Impact of pharmaceutical cocrystals: the effects on drug pharmacokinetics*. Expert Opinion on Drug Metabolism & Toxicology, 2014. **10**(9): p. 1255-1271.
2. Aitipamula, S., et al., *Polymorphs, Salts, and Cocrystals: What's in a Name?* Crystal Growth & Design, 2012. **12**(5): p. 2147-2152.
3. Qiao, N., et al., *Pharmaceutical cocrystals: An overview*. International Journal of Pharmaceutics, 2011. **419**(1–2): p. 1-11.
4. Nishimura, Y. and H. Hara, *Editorial: Drug Repositioning: Current Advances and Future Perspectives*. Frontiers in Pharmacology, 2018. **9**(1068).
5. Good, D.J. and N. Rodríguez-Hornedo, *Solubility Advantage of Pharmaceutical Cocrystals*. Crystal Growth & Design, 2009. **9**(5): p. 2252-2264.
6. Babu, N.J. and A. Nangia, *Solubility Advantage of Amorphous Drugs and Pharmaceutical Cocrystals*. Crystal Growth & Design, 2011. **11**(7): p. 2662-2679.
7. Childs, S.L., P. Kandi, and S.R. Lingireddy, *Formulation of a Danazol Cocrystal with Controlled Supersaturation Plays an Essential Role in Improving Bioavailability*. Molecular Pharmaceutics, 2013. **10**(8): p. 3112-3127.
8. Li, M., et al., *Investigation of the Effect of Hydroxypropyl Methylcellulose on the Phase Transformation and Release Profiles of Carbamazepine-Nicotinamide Cocrystal*. Pharmaceutical Research, 2014. **31**(9): p. 2312-2325.
9. Qiu, S., et al., *Role of polymers in solution and tablet-based carbamazepine cocrystal formulations*. CrystEngComm, 2016. **18**(15): p. 2664-2678.
10. Qiu, S. and M. Li, *Effects of coformers on phase transformation and release profiles of carbamazepine cocrystals in hydroxypropyl methylcellulose based matrix tablets*. International Journal of Pharmaceutics, 2015. **479**(1): p. 118-128.
11. Guo, M., et al., *Investigating the Influence of Polymers on Supersaturated Flufenamic Acid Cocrystal Solutions*. Molecular Pharmaceutics, 2016. **13**(9): p. 3292-3307.
12. Guo, M., et al., *Insight into Flufenamic Acid Cocrystal Dissolution in the Presence of a Polymer in Solution: from Single Crystal to Powder Dissolution*. Molecular Pharmaceutics, 2017. **14**(12): p. 4583-4596.
13. Guo, M., et al., *Investigating Permeation Behavior of Flufenamic Acid Cocrystals Using a Dissolution and Permeation System*. Molecular Pharmaceutics, 2018. **15**(9): p. 4257-4272.
14. Kirubakaran, P., et al., *Understanding the Effects of a Polymer on the Surface Dissolution of Pharmaceutical Cocrystals Using Combined Experimental and Molecular Dynamics Simulation Approaches*. Molecular Pharmaceutics, 2020. **17**(2): p. 517-529.
15. Shah, A.K. and S.A. Agnihotri, *Recent advances and novel strategies in pre-clinical formulation development: An overview*. Journal of Controlled Release, 2011. **156**(3): p. 281-296.
16. Hermans, A., et al., *Approaches for Establishing Clinically Relevant Dissolution Specifications for Immediate Release Solid Oral Dosage Forms*. The AAPS Journal, 2017. **19**(6): p. 1537-1549.
17. Agoram, B., W.S. Woltosz, and M.B. Bolger, *Predicting the impact of physiological and biochemical processes on oral drug bioavailability*. Advanced Drug Delivery Reviews, 2001. **50**: p. S41-S67.
18. Jamei, M., G.L. Dickinson, and A. Rostami-Hodjegan, *A Framework for Assessing Inter-individual Variability in Pharmacokinetics Using Virtual Human Populations*

- and Integrating General Knowledge of Physical Chemistry, Biology, Anatomy, Physiology and Genetics: A Tale of ‘Bottom-Up’ vs ‘Top-Down’ Recognition of Covariates. *Drug Metabolism and Pharmacokinetics*, 2009. **24**(1): p. 53-75.
19. Pathak, S.M., et al., *Model-Based Analysis of Biopharmaceutic Experiments To Improve Mechanistic Oral Absorption Modeling: An Integrated in Vitro in Vivo Extrapolation Perspective Using Ketoconazole as a Model Drug*. *Molecular Pharmaceutics*, 2017. **14**(12): p. 4305-4320.
 20. Kostewicz, E.S., et al., *PBPK models for the prediction of in vivo performance of oral dosage forms*. *European Journal of Pharmaceutical Sciences*, 2014. **57**: p. 300-321.
 21. Guiastrin, B., et al., *In Vitro and In Vivo Modeling of Hydroxypropyl Methylcellulose (HPMC) Matrix Tablet Erosion Under Fasting and Postprandial Status*. *Pharmaceutical Research*, 2017. **34**(4): p. 847-859.
 22. Sjögren, E., et al., *In silico predictions of gastrointestinal drug absorption in pharmaceutical product development: Application of the mechanistic absorption model GI-Sim*. *European Journal of Pharmaceutical Sciences*, 2013. **49**(4): p. 679-698.
 23. Sjögren, E., et al., *In vivo methods for drug absorption – Comparative physiologies, model selection, correlations with in vitro methods (IVIVC), and applications for formulation/API/excipient characterization including food effects*. *European Journal of Pharmaceutical Sciences*, 2014. **57**: p. 99-151.
 24. Kesisoglou, F. and A. Mitra, *Application of Absorption Modeling in Rational Design of Drug Product Under Quality-by-Design Paradigm*. *The AAPS Journal*, 2015. **17**(5): p. 1224-1236.
 25. Hens, B., et al., *In Silico Modeling Approach for the Evaluation of Gastrointestinal Dissolution, Supersaturation, and Precipitation of Posaconazole*. *Molecular Pharmaceutics*, 2017. **14**(12): p. 4321-4333.
 26. Zhang, X., et al., *Utility of Physiologically Based Absorption Modeling in Implementing Quality by Design in Drug Development*. *The AAPS Journal*, 2011. **13**(1): p. 59-71.
 27. Okumu, A., M. DiMaso, and R. Löbenberg, *Dynamic Dissolution Testing To Establish In Vitro/In Vivo Correlations for Montelukast Sodium, a Poorly Soluble Drug*. *Pharmaceutical Research*, 2008. **25**(12): p. 2778-2785.
 28. Parrott, N. and T. Lave, *Applications of Physiologically Based Absorption Models in Drug Discovery and Development*. *Molecular Pharmaceutics*, 2008. **5**(5): p. 760-775.
 29. Andreas, C.J., et al., *Mechanistic investigation of the negative food effect of modified release zolpidem*. *European Journal of Pharmaceutical Sciences*, 2017. **102**: p. 284-298.
 30. Riedmaier, A.E., et al., *Use of Physiologically Based Pharmacokinetic (PBPK) Modeling for Predicting Drug-Food Interactions: an Industry Perspective*. *The AAPS Journal*, 2020. **22**(6): p. 123.
 31. Jones, H.M., K. Mayawala, and P. Poulin, *Dose selection based on physiologically based pharmacokinetic (PBPK) approaches*. *The AAPS journal*, 2013. **15**(2): p. 377-387.
 32. Rowland Yeo, K., et al., *Physiologically based mechanistic modelling to predict complex drug–drug interactions involving simultaneous competitive and time-dependent enzyme inhibition by parent compound and its metabolite in both liver and gut—The effect of diltiazem on the time-course of exposure to triazolam*. *European Journal of Pharmaceutical Sciences*, 2010. **39**(5): p. 298-309.
 33. Nestorov, I., *Whole-body physiologically based pharmacokinetic models*. *Expert Opinion on Drug Metabolism & Toxicology*, 2007. **3**(2): p. 235-249.
 34. Clewell Iii, H.J., *Coupling of computer modeling with in vitro methodologies to reduce animal usage in toxicity testing*. *Toxicology Letters*, 1993. **68**(1): p. 101-117.

35. Isacchi, B., et al., *Artemisinin and artemisinin plus curcumin liposomal formulations: Enhanced antimalarial efficacy against Plasmodium berghei-infected mice*. European Journal of Pharmaceutics and Biopharmaceutics, 2012. **80**(3): p. 528-534.
36. Kaur, M., et al., *Artemisinin Cocrystals for Bioavailability Enhancement: Formulation Design and Role of the Polymeric Excipient* Molecular Pharmaceutics, 2021: p. accepted.
37. Kamau, E., et al., *Measurement of parasitological data by quantitative real-time PCR from controlled human malaria infection trials at the Walter Reed Army Institute of Research*. Malaria Journal, 2014. **13**(1): p. 288.
38. Manser, M., et al., *Estimating the parasitaemia of Plasmodium falciparum: experience from a national EQA scheme*. Malaria journal, 2013. **12**: p. 428-428.
39. Wong, J.W. and K.H. Yuen, *Improved oral bioavailability of artemisinin through inclusion complexation with β - and γ -cyclodextrins*. International Journal of Pharmaceutics, 2001. **227**(1): p. 177-185.
40. Gordi, T., et al., *Artemisinin pharmacokinetics and efficacy in uncomplicated-malaria patients treated with two different dosage regimens*. Antimicrobial agents and chemotherapy, 2002. **46**(4): p. 1026-1031.
41. Elsherbiny, D.A., et al., *A model based assessment of the CYP2B6 and CYP2C19 inductive properties by artemisinin antimalarials: implications for combination regimens*. Journal of Pharmacokinetics and Pharmacodynamics, 2008. **35**(2): p. 203-217.
42. Simonsson, U.S.H., et al., *Artemisinin autoinduction is caused by involvement of cytochrome P450 2B6 but not 2C9*. Clinical Pharmacology & Therapeutics, 2003. **74**(1): p. 32-43.
43. Svensson, U.S.H., et al., *Artemisinin induces omeprazole metabolism in human beings*. Clinical Pharmacology & Therapeutics, 1998. **64**(2): p. 160-167.
44. Simonsson, U.S.H., et al., *In vivo and mechanistic evidence of nuclear receptor CAR induction by artemisinin*. European Journal of Clinical Investigation, 2006. **36**(9): p. 647-653.
45. Jamei, M., et al., *The Simcyp® Population-based ADME Simulator*. Expert Opinion on Drug Metabolism & Toxicology, 2009. **5**(2): p. 211-223.
46. Jamei, M., et al., *The Simcyp Population Based Simulator: Architecture, Implementation, and Quality Assurance*. In Silico Pharmacology, 2013. **1**(1): p. 9.
47. Isacchi, B., et al., *Artemisinin and artemisinin plus curcumin liposomal formulations: enhanced antimalarial efficacy against Plasmodium berghei-infected mice*. Eur J Pharm Biopharm, 2012. **80**(3): p. 528-34.
48. Lacerda-Queiroz, N., et al., *Plasmodium berghei NK65 induces cerebral leukocyte recruitment in vivo: An intravital microscopic study*. Acta Tropica, 2011. **120**(1): p. 31-39.
49. Organization, W.H., *Guidelines for the treatment of malaria 2015*, WHO Press: Geneva.
50. De Niz, M., et al., *Progress in imaging methods: insights gained into Plasmodium biology*. Nature Reviews Microbiology, 2017. **15**(1): p. 37-54.
51. Gordi, T., et al., *A semiphysiological pharmacokinetic model for artemisinin in healthy subjects incorporating autoinduction of metabolism and saturable first-pass hepatic extraction*. Br J Clin Pharmacol, 2005. **59**(2): p. 189-98.
52. Ashton, M., *Quantitative in vivo and in vitro sex differences in artemisinin metabolism in rat*. Xenobiotica, 1999. **29**(2): p. 195-204.

53. Svensson, U.S.H., et al., *High In Situ Rat Intestinal Permeability of Artemisinin Unaffected by Multiple Dosing and with No Evidence of P-glycoprotein Involvement*. Drug Metabolism and Disposition, 1999. **27**(2): p. 227-232.
54. Morris, C.A., et al., *Review of the clinical pharmacokinetics of artesunate and its active metabolite dihydroartemisinin following intravenous, intramuscular, oral or rectal administration*. Malaria Journal, 2011. **10**(1): p. 263.
55. Sidhu, J.S., et al., *Artemisinin population pharmacokinetics in children and adults with uncomplicated falciparum malaria*. British journal of clinical pharmacology, 1998. **45**(4): p. 347-354.
56. Gupta, S., U.S.H. Svensson, and M. Ashton, *In vitro evidence for auto-induction of artemisinin metabolism in the rat*. European Journal of Drug Metabolism and Pharmacokinetics, 2001. **26**(3): p. 173-178.
57. Dai, T., et al., *Comparison of in vitro/in vivo blood distribution and pharmacokinetics of artemisinin, artemether and dihydroartemisinin in rats*. Journal of Pharmaceutical and Biomedical Analysis, 2019. **162**: p. 140-148.
58. Gordi, T., et al., *Use of saliva and capillary blood samples as substitutes for venous blood sampling in pharmacokinetic investigations of artemisinin*. European Journal of Clinical Pharmacology, 2000. **56**(8): p. 561-566.
59. Klayman, D., *Qinghaosu (artemisinin): an antimalarial drug from China*. Science, 1985. **228**(4703): p. 1049-1055.
60. Prieto Garcia, L., et al., *Physiologically Based Pharmacokinetic Model of Itraconazole and Two of Its Metabolites to Improve the Predictions and the Mechanistic Understanding of CYP3A4 Drug-Drug Interactions*. Drug Metabolism and Disposition, 2018. **46**(10): p. 1420-1433.
61. Patel, K., et al., *Predicting the parasite killing effect of artemisinin combination therapy in a murine malaria model*. Journal of Antimicrobial Chemotherapy, 2014. **69**(8): p. 2155-2163.
62. Kumari, A., et al., *Current scenario of artemisinin and its analogues for antimalarial activity*. European Journal of Medicinal Chemistry, 2019. **163**: p. 804-829.
63. Woodrow, C.J., R.K. Haynes, and S. Krishna, *Artemisinins*. Postgraduate Medical Journal, 2005. **81**(952): p. 71-78.
64. Stanton, M.K., et al., *Improved pharmacokinetics of AMG 517 through co-crystallization part 2: analysis of 12 carboxylic acid co-crystals*. J Pharm Sci, 2011. **100**(7): p. 2734-43.
65. Stanton, M.K., et al., *Improved pharmacokinetics of AMG 517 through co-crystallization. Part 1: comparison of two acids with corresponding amide co-crystals*. J Pharm Sci, 2010. **99**(9): p. 3769-78.
66. Sager, J.E., et al., *Physiologically Based Pharmacokinetic (PBPK) Modeling and Simulation Approaches: A Systematic Review of Published Models, Applications, and Model Verification*. Drug metabolism and disposition: the biological fate of chemicals, 2015. **43**(11): p. 1823-1837.